Inhibition of ULK1/2 and KRAS^{G12C} controls tumor growth in preclinical models of lung cancer

Phaedra C. Ghazi[1,2], Kayla T. O'Toole[1,2], Sanjana Srinivas Boggaram[1,2], Michael T. Scherzer[1,2], Mark R. Silvis[1,2], Yun Zhang[3], Madhumita Bogdan[4], Bryan D. Smith[4], Guillermina Lozano[3], Daniel L. Flynn[4], Eric L. Snyder[1,2,5], Conan G. Kinsey[1,2,6] and Martin McMahon[1,2,7,*]

[1.] Department of Oncological Sciences, University of Utah, Salt Lake City, UT.
[2.] Huntsman Cancer Institute, University of Utah, Salt Lake City, UT.
[3.] Department of Genetics, University of Texas MD Anderson Cancer Center, Houston, TX
[4.] Deciphera Pharmaceuticals LLC, 643 Massachusetts St, Lawrence, Kansas.
[5] Department of Pathology, University of Utah, Salt Lake City, UT.
[6.] Department of Internal Medicine, Division of Medical Oncology, University of Utah, Salt Lake City, UT.
[7.] Department of Dermatology, University of Utah, Salt Lake City, UT.

* Corresponding Author

Martin McMahon, PhD
Huntsman Cancer Inst., Dept of Dermatology & Dept. of Oncological Sciences,
University of Utah,
2000 Circle of Hope Drive, HCI-RS-2725
Salt Lake City, UT 84112
(801) 213 5790
Email: martin.mcmahon@hci.utah.edu

Author Contributions: PCG, MM, MB, BDS, and DLF designed the experiments; PCG and MM analyzed the data; PCG performed the majority of the experiments; KTO assisted with immunoblotting; MRS performed *in vitro* synergy assays; SSB and MTS assisted with *in vivo* animal studies; ELS performed histopathological analysis; PCG and MM wrote the manuscript; all authors reviewed and edited the manuscript.

Competing Interest Statement: Research described here was supported through a Sponsored Research Agreement between the University of Utah and Deciphera Pharmaceuticals, LLC and awarded to MM and CGK.

Keywords: KRAS, ULK, LKB1, TP53, Autophagy, Genetically-engineered mouse models of KRAS^{G12C}-driven lung cancer

ABSTRACT

Mutational activation of *KRAS* occurs commonly in lung carcinogenesis and, with the recent FDA approval of covalent inhibitors of KRAS^{G12C} such as sotorasib or adagrasib, KRAS oncoproteins are important pharmacological targets in non-small cell lung cancer (NSCLC). However, not all KRAS^{G12C}-driven NSCLCs respond to these inhibitors, and the emergence of drug resistance in those patients that do respond can be rapid and pleiotropic. Hence, based on a backbone of covalent inhibition of KRAS^{G12C}, efforts are underway to develop effective combination therapies. Here we report that inhibition of KRAS^{G12C} signaling increases autophagy in KRAS^{G12C} expressing lung cancer cells. Moreover, the combination of DCC-3116, a selective ULK1/2 inhibitor, plus sotorasib displays cooperative/synergistic suppression of human KRAS^{G12C}-driven lung cancer cell proliferation *in vitro* and superior tumor control *in vivo*. Additionally, in genetically engineered mouse models of KRAS^{G12C}-driven NSCLC, inhibition of either KRAS^{G12C} or ULK1/2 decreases tumor burden and increases mouse survival. Consequently, these data suggest that ULK1/2-mediated autophagy is a pharmacologically actionable cytoprotective stress response to inhibition of KRAS^{G12C} in lung cancer.

INTRODUCTION

Lung adenocarcinoma (LUAD) is responsible for ~50,000 deaths/year in the USA. Amongst the most common genetic drivers of LUAD are mutations in *KRAS* that encode KRAS-4A and -4B oncoproteins among which the substitution of cysteine for glycine at codon 12 ($KRAS^{G12C}$) is the most common mutation and is associated with exposure to tobacco smoke[1,2]. For many years, RAS (H-, K- or N) oncoproteins were considered undruggable until the seminal work of Ostrem et al. that demonstrated the feasibility of developing covalent inhibitors of $KRAS^{G12C}$ that bind into the Switch II pocket of $KRAS^{G12C}$-GDP and derivatize the reactive thiol of cysteine 12 [3–5].

We and others have previously reported that inhibition of RAS>RAF>MEK>ERK signaling in melanoma or pancreatic cancer cells elicits increased autophagy, an intracellular macromolecule and organelle recycling mechanism, through the LKB1>AMPK>ULK1 signaling axis[6–9]. Liver kinase B1 (LKB1) activates AMP kinases in response to cellular nutrient changes to maintain homeostasis[10]. However, induction of autophagy has also been reported in response to MEK inhibition in models of $KRAS^{G12D}$-driven lung cancer with loss of LKB1 expression[11], suggesting that LKB1 is dispensable for increases in autophagy in lung cancer. LKB1 silencing is frequently observed in patients with KRAS-driven lung cancer, and such patients exhibit decreased overall survival and are more refractory to current therapeutic treatments than in LKB1 proficient KRAS-driven lung cancers[12,13]. With the advent of FDA-approved covalent $KRAS^{G12C}$ inhibitors, it is imperative to investigate if autophagy occurs following inhibition of $KRAS^{G12C}$ signaling, especially since MEK inhibitors offer little clinical benefit accompanied by toxicity to lung cancer patients[14]. This prompted us to explore if treatment with sotorasib leads to an increase in autophagy in $KRAS^{G12C}$ mutant lung cancer cells with and without the expression of LKB1.

At present, the only FDA-approved therapeutics that inhibit autophagy are the 4-amino-quinolone lysosomal inhibitors chloroquine (CQ) and hydroxychloroquine (HCQ)[15]. Originally approved for treating malaria, HCQ acts by inhibiting Toll-like receptors[16]. It was also reported that HCQ inhibits acidification of the lysosome, thereby inhibiting auto-lysosome activity, although the precise mechanism of this remains obscure[17–19]. Clinically, high concentrations of HCQ are required to achieve modest inhibition of autophagy in patients, suggesting that the inhibitory potency of these compounds may limit clinical responses. Indeed, co-targeting lysosomal function in combination with RAS-driven signaling has recently been tested in RAS-driven cancers in several clinical trials[8,9,20] (clinicaltrials.gov: NCT04214418, NCT04132505, NCT04386057, NCT04145297). However, there is a lack of clinical investigation on targeting autophagy with selective autophagy inhibitors in patients.

Autophagy is a complex intracellular recycling process important for maintaining cellular homeostasis under stressed conditions. The genetics and biochemistry of autophagy, first revealed in

yeast[21], indicate numerous points of regulation of which the initiation and formation of the autophagosome, as well as the fusion of the autophagosome to the lysosome are of key importance.[21,22] ULK1/2 are protein serine/threonine kinases that form a complex with FIP200, ATG13 and ATG101, which integrates upstream signals from mTORC1 and AMPK energy-sensing pathways[22]. Upon activation, ULK1/2 phosphorylate a number of substrates including ATG13 (at serine 318, pS318) to initiate the formation of autophagosomes[22]. There remains interest in the development of selective inhibitors of autophagy for use in a number of disease indications. [23] DCC-3116 is one such "switch-control" ULK1/2 inhibitor, which is currently in Phase 1/2 clinical trials either as a monotherapy or in combination with inhibitors of $KRAS^{G12C}$, MEK1/2 or EGFR (NCT04892017 & NCT05957367).

Here, we test the anti-tumor effects of DCC-3116 against preclinical models of $KRAS^{G12C}$-driven lung cancer either alone or in combination with sotorasib. We observed that cultured $KRAS^{G12C}$-driven lung cancer cells increase autophagy in response to inhibition of $KRAS^{G12C}$>RAF>MEK>ERK signaling. In addition, combined inhibition of $KRAS^{G12C}$ plus ULK1/2 leads to decreased cell proliferation and tumor growth. Moreover, using GEM models of ether $KRAS^{G12C}$/$TP53^{R172H}$- or $KRAS^{G12C}$/$LKB1^{Null}$-driven lung cancer[24], we demonstrate that LKB1 is dispensable for increases in autophagy following $KRAS^{G12C}$ inhibition. Furthermore, LKB1 silencing diminishes the sensitivity of $KRAS^{G12C}$/$LKB1^{Null}$-driven lung cancer perhaps through the emergence of mixed adeno/squamous cell carcinomas and mucinous adenocarcinomas. Adeno/squamous carcinomas are observed in up to 4% of lung cancers and the emergence of these tumors is observed as a resistance mechanism to current therapeutics in lung cancer patients[25]. Patients with ASC tend to exhibit substantially decreased overall survival compared to patients with adenocarcinomas or squamous carcinomas[26]. These data suggest that $KRAS^{G12C}$ mutant lung tumors with adeno/squamous pathology may not respond to $KRAS^{G12C}$ or ULK inhibition. Clinical acquired resistance to sotorasib and adagrasib is emerging in $KRAS^{G12C}$ mutant lung cancer patients[27–33]. Here, we demonstrate that $KRAS^{G12C}$/$LKB1^{Null}$-driven lung cancer cells that acquire resistance to sotorasib increase expression of RAS>RAF>MEK>ERK signaling, and no longer increase autophagy after sotorasib treatment. These cells do induce autophagy after MEK1/2 inhibition and decrease cellular proliferation and viability after treatment with trametinib, suggesting that sotorasib-resistant cells are still vulnerable to downstream $KRAS^{G12C}$ signaling inhibition.

RESULTS

Human $KRAS^{G12C}$-driven lung cancer cells are sensitive to co-inhibition of $KRAS^{G12C}$ and ULK1/2

To determine if direct inhibition of $KRAS^{G12C}$ in lung cancer cells influences autophagy, human $KRAS^{G12X}$-driven lung cancer cell lines were engineered to express a chimeric fluorescent autophagy reporter (FAR) comprised of mCherry fused to EGFP fused to LC3[8,34]. LC3 targets the chimeric FAR to

the autophagosome where the pH sensitive EGFP moiety is quenched in the acidic environment of the autolysosome (pH<5). Hence, an increase in the ratio of mCherry:EGFP fluorescence is indicative of increased autophagy[8,34]. All KRAS^{G12C}-driven lung cancer cells displayed dose-dependent increases in autophagy following sotorasib treatment as indicated by an increase in the mCherry:EGFP ratio detected in live cells (Figs. 1A-C, Figs. S1A-D). Since sotorasib is reported to bind to >300 proteins, we ruled out non-specific effects of sotorasib on autophagy, by treating a KRAS^{G12V}-driven NSCLC cell line (COR-L23) with sotorasib, which failed to show any change in mCherry:EGFP fluorescence (Fig. S1E) [35]. Moreover, as predicted by previous experiments, all KRAS^{G12X}-driven NSCLC cell lines displayed a dose-dependent increase in autophagy following treatment with trametinib, a MEK1/2 inhibitor (Figs. S1F-J)[8].

Next, we tested the effects of DCC-3116 on autophagy in KRAS^{G12C}-driven NSCLC cell lines. As anticipated, DCC-3116 inhibited both basal and sotorasib-induced autophagy in all KRAS^{G12C}-driven cell lines as assessed using the FAR (Figs. 1A-C). In addition, DCC-3116 treatment, either alone or in combination with sotorasib, led to decreased pS318-ATG13, one of ULK1's immediate downstream substrate (Figs. S2A-C). To test if DCC-3116 might show additive or synergistic anti-proliferative effects when combined with sotorasib, human KRAS^{G12C}-driven NSCLC cells were treated with varying concentrations of both drugs for 72 hours with cell proliferation assessed using a cell viability assay. Interestingly, we observed synergistic anti-proliferative effects of DCC-3116 plus sotorasib in NCI-H2122 and Calu-1 cell lines (Figs. 1G-H), but not in NCI-H358 cells, which are noted to be exquisitely sensitive to single agent sotorasib (Fig. 1I). Using the Incucyte platform, we measured cell proliferation over time and noted that the combination of sotorasib plus DCC-3116 was superior to either single agent in NCI-H2122 and Calu-1 cells (Figs. 1D-E, Figs. S2D-E), but not in NCI-H358 cells (Fig, 1F, Fig. S2F). Intriguingly, we observed consistent inhibition of NCI-H358 cell proliferation with single agent DCC-3116 (Fig. 1F, Fig. S2F).

We next proceeded to test the anti-tumor effects of DCC-3116, either alone or in combination with sostorasib, against xenografted tumors derived from injection of NCI-H2122, Calu-1 or NCI-H358 cells into immunocompromised mice. Here, we observed clear cooperation of sotorasib plus DCC-3116 in tumors derived from NCI-H2122 and Calu-1 cells (Figs. 1J-K) but not from NCI-H358 cells, which are noted for their sensitivity to low-concentrations of sotorasib (Fig. 1L). To confirm the inhibitory activity of sotorasib in the cell lines used, cell extracts of control vs. sotorasib treated NSCLC cells were immunoblotted for phospho-ERK1/2. As expected, pERK1/2 was decreased in all cell lines following 2 hours of sotorasib treatment (Fig. S2G-I). In addition, we detected by immunoblotting the expected electrophoretic mobility shift of KRAS^{G12C}, which is indicative of covalent binding of sotorasib (561 daltons) to cysteine 12 of KRAS^{G12C} (Figs. S2G-I).[27]

Genetic inhibition of ULK1 decreases autophagy and cooperates with sotorasib to reduce cell viability

As an alternate way to assess the role of ULK1/2 in sotorasib-induced autophagy, we conditionally expressed a kinase-inactive, dominant negative form of ULK1 ($ULK1^{K46N}$) under the control of a tetracycline transactivator (Tet^{ON})[36]. Doxycycline treatment of NCI-H2122/Tet^{ON}::$ULK1^{K46N}$ cells led to a substantial increase in total ULK1 expression within 8 hours, which could be inferred to also be phosphorylated at known sites (pS555 and pS747) of regulatory phosphorylation of ULK1 (Figs. 2A-B). As anticipated, expression of $ULK1^{K46N}$ led to decreased phosphorylation of pS318-ATG13 in a manner comparable to treatment with DCC-3116 (Fig. 2C). In addition, expression of $ULK1^{K46N}$ led to a decrease in both basal and sotorasib-induced autophagy as assessed using the FAR. Finally, expression of $ULK1^{K46N}$ displayed synergistic anti-proliferative effects in NCI-H2122 cells when combined with sotorasib for 48 hours, suggesting that both genetic and pharmacological inhibition of ULK1 signaling had similar effects on NCI-H2122 cells (Fig. 2E).

Either LKB1 silencing or expression of dominant-negative $TP53^{R172H}$ cooperates with $KRAS^{G12C}$-in GEM models of lung cancer.

To complement the use of cultured human lung cancer cells, and to further test how additional genetic alterations influence $KRAS^{G12C}$-driven lung tumor progression and treatment response, we generated genetically engineered mouse (GEM) models of $KRAS^{G12C}$-driven lung cancer. To that end, we crossed *Kras*$^{LSL\text{-}G12C/+}$ (*K*)[24] mice to either: 1. *Stk11*$^{fl/fl}$ [37]mice to generate *KL* mice or; 2. *Trp53*$^{wm\text{-}R172H}$ to generate *KP* mice[38]. Intranasal administration of an adenovirus encoding CRE recombinase under the control of a CMV promoter (Ad-CMV-CRE) to *KL* mice initiates expression of $KRAS^{G12C}$ plus silencing of LKB1 in alveolar type 2 (AT2) cells. Similar treatment of *KP* mice initiates expression of $KRAS^{G12C}$ plus dominant-negative $TP53^{R172H}$ in AT2 cells (Fig. 3A, Fig. S3A, Table 1). At euthanasia, 14 weeks post-initiation (p.i.), compared to *Kras*$^{LSL\text{-}G12C/+}$ *(K)* mice, *KL* and *KP* mice displayed both accelerated lung cancer formation (Fig. 3B) and increased tumor burden (Fig. 3C). Histopathological analysis of H&E stained sections of $KRAS^{G12C}$ only-driven lung tumors, also at 14 weeks p.i., indicated that they comprised mainly of atypical adenomatous hyperplasia (AAH) and low-grade small lung adenocarcinomas. $KRAS^{G12C}$/$LKB1^{Null}$-driven lung tumors comprised AHH, adenocarcinomas, adenosquamous carcinomas (ASC) and mucinous adenocarcinomas. Finally, $KRAS^{G12C}$/$TP53^{R172H}$-driven lung tumors consisted of AAH and a mix of low- and higher-grade lung adenocarcinomas (Fig. S3B). Immunohistochemical analysis of tumor sections indicated that phospho-ERK1/2 (pERK1/2) was detected in $KRAS^{G12C}$-driven lung tumors regardless of cooperating alterations in LKB1 or TP53 (Fig. 3D). However, the intensity of pERK1/2 staining across all three GEM models, and even between lesions in the same lung lobe (Fig. S3C) displayed substantial variability. Moreover, phospho-AKT1-3 (a surrogate for activation of PI3'-kinase signaling) was low across all $KRAS^{G12C}$-driven lung tumors, albeit that some individual cells in tumors had readily detected pAKT1-3 (Fig. S3D). Similar analysis confirmed the absence of LKB1 in $KRAS^{G12C}$/$LKB1^{Null}$-driven lung tumors, but its presence in $KRAS^{G12C}$ only and $KRAS^{G12C}$/$TP53^{R172H}$-driven lung tumors. Similarly,

KRAS^{G12C}/TP53^{R172H}-driven lung tumors displayed elevated expression of TP53 that was not observed in KRAS^{G12C} only or in KRAS^{G12C}/LKB1^{Null}-driven lung tumors (Fig. 3D). Previously published data demonstrated that KRAS-driven lung cancer cells occasionally suppress expression of NK2 homeobox 2 (NKX2.1), a master-regulatory transcription factor required for normal lung development[39]. In addition, KRAS-driven but NKX2.1 deficient lung tumors display a mucinous adenocarcinoma pathology and other transcriptional features of a pulmonary-to-gastric lineage switch [40]. Although mucinous adenocarcinomas were detected in lung sections from KL mice (Fig. 3D), these KRAS^{G12C}/LKB1^{Null} tumor cells retained expression of NKX2.1 (Fig. 3D, Fig. S3E), and some cells also expressed the gastrointestinal transcription factor HNF4α (Fig. S3E). Finally, we assessed expression of the AT2 specific pro-surfactant protein C (SPC), a surfactant important for the function of normal lung[41], and noted its uniform expression in KRAS^{G12C} only driven lung tumors, but more variable expression in KRAS^{G12C}/LKB1^{Null}- and KRAS^{G12C}/TP53^{R172H}-driven lung tumors (Fig. 3D).

Anti-tumor effects of DCC-3116 and sotorasib either alone or in combination in GEM models of KRAS^{G12C}-driven lung cancer

The importance of autophagy in the initiation and/or progression of KRAS- or BRAF-driven lung cancer was revealed through analysis of GEM models in which deletion of key autophagy genes (Atg5 or Atg7) accompanied the initiation of oncoprotein expression[42–46]. Hence, we tested if DCC-3116 mediated inhibition of ULK1/2, starting at tumor initiation in *KL* mice, would inhibit tumor growth. Therefore, *KL* were initiated with Ad-CMV-CRE and then, starting 2 days p.i., treated with either vehicle or DCC-3116 (using a chow formulation) for 12 weeks (Fig. 4A) at which time mice were euthanized for analysis. DCC-3116 treated *KL* mice displayed significantly decreased tumor burden compared to control *KL* mice (Figs. 4B-C).

To test if combined inhibition of KRAS^{G12C} plus ULK1/2 would inhibit growth of established KRAS^{G12C}/LKB1^{Null} lung tumors, tumor-bearing *KL* mice at 10 weeks p.i. were administered sotorasib or DCC-3116 either alone or in combination for 8 weeks or until the mice met pre-determined euthanasia endpoints (Fig. 4D). Compared to vehicle, all three treatments significantly increased the survival of tumor-bearing *KL* mice (Fig. 4E). Although there was a trend towards improved survival of *KL* mice treated with the combination of sotorasib plus DCC-3116, these differences were not statistically significant (Fig. 4E). We also utilized micro-computed tomography (microCT) to monitor the response of tumors[47] that were large enough to be detected throughout drug treatment (Fig. S4A). As expected, lung tumors in vehicle treated mice rapidly increased in size (Fig. S4A). The growth of KRAS^{G12C}/LKB1^{Null} tumors in mice treated with sotorasib, DCC-3116 or the combination was delayed compared to those in vehicle treated mice, but tumors ultimately progressed on treatment (Fig. S4). However, some lung tumors in mice treated with the sotorasib plus DCC-3116 drug combination did not appear to change their size over the course of treatment (Fig. S4A). Throughout the course of treatment, we observed

substantial (≥20%) weight loss in four out of five sotorasib only treated mice and one combination treated mouse that reached our euthanasia criteria (Fig. S4B). Following euthanasia, we performed immunohistochemical analysis on lung sections from control vs drug treated mice. In *KL* mice treated with sotorasib, either alone or in combination with DCC-3116, we noted a predominance of ASC and mucinous adenocarcinomas at the expense of AAH and adenocarcinoma (Fig. S4C). These results suggest that $KRAS^{G12C}$/$LKB1^{Null}$-driven ASC or mucinous adenocarcinomas may be less sensitive to sotorasib treatment (Figs. S4A,C). Intriguingly, single-agent DCC-3116 treatment also slowed the growth of established tumors compared to vehicle treatment (Fig. S4A), but this did not inhibit the growth of AAH or adenocarcinomas (Fig. S4C). Immunohistochemistry revealed the expected decrease in pERK1/2 and pAKT1-3 staining in tumors treated with sotorasib, either alone or in combination with DCC-3116, compared to mice treated with vehicle or single-agent DCC-3116 alone (Figs. 4G-I). NKX2.1 expression was detected in all lung tumors regardless of the treatment group (Fig. 4G). Finally, many mice, regardless of the treatment type, developed lung tumors with the aforementioned mucinous adenocarcinoma phenotype, expressing HNF4α and stained postitive for various mucins (Alcian-Blue/PAS-positive) (Fig. 4G).

To further compare and contrast the effects of sotorasib and DCC-3116, either alone or in combination in GEM models of lung cancer and because of noted correlations between loss of LKB1 and insensitivity of cancers to various types of therapy, we employed our *KP* mouse model. [12,48] $KRAS^{G12C}$/$TP53^{R172H}$-driven lung tumorigenesis was initiated in adult *KP* mice and at 10 weeks p.i. tumor bearing mice were treated with: 1. Vehicle control; 2. Sotorasib; 3. DCC-3116 or; 4. Combination of sotorasib plus DCC-3116 for 4 weeks (Fig. 5A) at which time mice were euthanized for analysis as described above. Interestingly, compared to control, there was a significant reduction in lung tumor burden in response to all three treatments (Fig. 5B). In addition, in all sotorasib treated mice, either alone or in combination with DCC-3116, regression of pre-existing lung tumors was detected by microCT scanning (Fig. 5C, Fig. S5). In mice treated with single agent DCC-3116, although an overall reduction in tumor burden was observed, some tumors detectable by microCT scanning continued to increase in size throughout treatment (Fig. 5B, Fig. S5). Moreover, in this experiment, we noted no weight loss in mice in any of the three treatment groups (Fig. 5C). Immunohistochemical analysis of lung sections from mice again revealed decreased pERK1/2 in mice treated with sotorasib either alone or in combination with DCC-3116, although pERK1/2 was detected in some areas of the lung (Figs. 5D-E). Vehicle treated $KRAS^{G12C}$/$TP53^{R172H}$-driven lung tumors had detectable pAKT, which was decreased by all three treatments (Figs. 5D, F). Finally, all tumors displayed expression of NKX2.1 that was not substantially altered by drug treatment (Fig. 5D).

_KL_ lung-cancer-derived cells that acquire resistance to sotorasib increase RAS and pERK1/2 expression and do not increase autophagy after sotorasib treatment

To complement our *in vivo* work with GEM models and to better understand how acquired sotorasib resistance influences autophagy and treatment sensitivity, we generated $KRAS^{G12C}$/$LKB1^{Null}$-lung cancer-derived cell lines from suitably manipulated, drug naive KL mice. As expected, parental KL70 cells are sensitive to the anti-proliferative effects of both sotorasib and the MEK1/2 inhibitor, trametinib (Figs. 6A-D). In addition, pERK1/2 also is inhibited by both sotorasib and trametinib (Fig. 6A). Next, we generated a sotorasib-resistant (SR) $KRAS^{G12C}$/$LKB1^{Null}$-driven lung cancer cell line by culturing parental KL70 cells over 12 weeks in gradually increasing concentrations of sotorasib until a resistant population emerged ($KL70^{SR}$ cells). $KL70^{SR}$ cells were entirely resistant to the anti-proliferative effects of sotorasib but remained sensitive to trametinib (Fig. D). Consistent with this, the level of pERK1/2 was sotorasib resistant but trametinib sensitive (Fig. 6A). Indeed, $KL70^{SR}$ cells had a higher baseline level of both RAS and pERK1/2 expression compared to parental KL70 cells, which might explain their more rapid baseline proliferation (Fig. 6D).

We next tested differences in baseline and drug-induced autophagy in KL70 and $KL70^{SR}$ cells using the fluorescent autophagy reporter. As expected based on analysis of human $KRAS^{G12C}$-driven lung cancer cells, KL70 cells increased autophagy in response to either sotorasib or trametinib treatment, a further demonstration that LKB1 is not required for increased autophagy in response to inhibition of $KRAS^{G12C}$>RAF>MEK>ERK inhibition (Fig. 6E). $KL70^{SR}$ cells treated with sotorasib displayed little induction of autophagy (Fig. 6E). However, trametinib elicited a robust induction of autophagy in $KL70^{SR}$ cells (Fig. 6E), further suggesting that changes in autophagy levels are correlated to pERK1/2 levels in the cell. Because sotorasib did not induce autophagy in the $KL70^{SR}$ cells, it was not clear if the addition of an autophagy inhibitor would decrease cell viability in the sotorasib-resistant cells. Cell viability was measured after 72 hours of drug treatment in the KL70 and $KL70^{SR}$ cell lines (Fig. 6 F-I). The combination of sotorasib and DCC-3116 did not lead to decreases in cell viability in the $KL70^{SR}$ cells (Fig. 6 H). We next tested if there were any synergist decreases in cell viability with the combination of trametinib and DCC-3116 because there was a robust increase in autophagy levels with trametinib treatment in the $KL70^{SR}$ cells. $KL70^{SR}$ cells are exquisitely sensitive to trametinib at very low concentrations and therefor little synergy was observed with the tested concentrations (Fig. I).

DISCUSSION

Cancer cells exhibit increased autophagy in response to a variety of cellular stresses including nutrient deprivation or the application of pathway-targeted therapy, thereby allowing cancer cells to recycle a wide variety of macromolecules and organelles to promote cell viability.[8,11] Moreover, GEM models of lung or pancreatic cancer indicate that cancer cells employ autophagy - both cancer cell autonomous and from the mouse as a whole - at a several stages of cancer progression[46,49]. Recently,

we and others have demonstrated that many RAS-driven cancer cells display increased autophagy in response to blockade of RAS>RAF>MEK>ERK signaling [8,9,11]. Moreover, in our work, combined inhibition of MEK1/2 (with trametinib) plus inhibition of lysosome function (with CQ or HCQ) displayed synergistic anti-proliferative activity *in vitro*, superior tumor control (compared to the single agents or standard of care) in cell line- or patient-derived xenografts (CDX or PDX) models of pancreatic cancer and, in one patient with advanced pancreatic cancer, there was evidence of anti-tumor activity of the combination of trametinib plus hydroxychloroquine[8]. These data (and others) have led to a number of clinical trials, some of which are ongoing (clinicaltrials.gov: NCT04214418, NCT04132505, NCT04386057, NCT04145297). Here we expand these observations using preclinical models of $KRAS^{G12C}$-driven lung cancer. The management of this disease has been transformed by FDA approval of adagrasib and sotorasib, covalent inhibitors of the $KRAS^{G12C}$ oncoprotein[27–29]. However, as is generally true for single-agent pathway-targeted cancer therapy, the emergence of drug resistant disease can be rapid and pleiotropic[50]. Our data suggest that combined inhibition of $KRAS^{G12C}$ plus autophagy may have superior activity against $KRAS^{G12C}$-driven lung cancer. These data are in accord with a recent study in which HCQ-mediated inhibition of lysosome function sensitized a $KRAS^{G12D}$/$LKB1^{Null}$-driven GEM model of lung cancer to MEK1/2 inhibition [11]. An interesting aspect of these results is the apparent dispensability of LKB1 for the induction of autophagy in response to inhibition of KRAS signaling. Our work and that of others had concluded that LKB1 was important for trametinib-induced autophagy in pancreatic cancer cells, but this new data argues that LKB1 is not an obligate requirement for autophagy induction[8]. Co-alterations in KRAS plus LKB1 are frequent in lung cancer and patients with these alterations are reported to display resistance to current therapeutic options such as chemotherapy and/or immunotherapy[13,51,52]. In addition, and perhaps surprisingly, we noted that DCC-3116 had substantial single-agent activity against $KRAS^{G12C}$-driven lung cancers in GEM models. Importantly, previous studies have demonstrated that combined inhibition of MEK1/2 plus autophagy does not lead to synergistic or cooperative decreases in cell proliferation or tumor growth in a GEM model of $KRAS^{G12D}$/$TP53^{Null}$-driven lung cancer in which LKB1 expression is retained[11] . Here, we show that combined inhibition of $KRAS^{G12C}$ plus ULK1/2 in Calu-1 cells ($KRAS^{G12C}$/$LKB1^{WT}$/$TP53^{null}$) decreased cell proliferation and tumor growth and that this combination was more effective than either single agent. Our findings demonstrate that inhibition of both $KRAS^{G12C}$ plus ULK1/2 kinases is synergistic in $KRAS^{G12C}$ mutant lung cancer cells with wild-type LKB1 expression but loss of TP53 expression. The difference between these findings could be due to the difference in KRAS missense mutation driving lung tumorigenesis or differences between inhibiting autophagy with a 4-aminoquiniolone such hydroxychloroquine and DCC-3116 mediated inhibition of ULK1/2. Indeed, since HCQ inhibits lysosome function, it might inhibit cellular recycling of substrates acquired by micropinocytosis, whereas ULK1/2 inhibition should be specific for autophagic recycling of intracellular substrates. Hence, this work supports the hypothesis that patients with $KRAS^{G12C}$-driven lung cancers may benefit from treatment with the combination of $KRAS^{G12C}$ plus ULK1/2 inhibitors. To that end, there

is an ongoing clinical trial enrolling patients with KRAS^{G12C}-driven cancers to test the combination of sotorasib plus DCC-3116 (NCT04892017).

Autophagy is reported to promote lung tumor progression by supporting tumor energy production[43]. Others have demonstrated that silencing of Autophagy-Related 7 (ATG7) expression, a protein essential for autophagy, in KRAS^{G12D}/LKB1^{null} driven tumors at the time of tumor initiation substantially diminishes lung tumor burden[43]. Our study suggests that pharmacological inhibition of ULK1/2 kinase activity starting at tumor initiation also significantly reduces growth of KRAS^{G12C}/LKB1^{null} lung tumors. Together, these data suggest that both ATG7 and ULK1/2 kinases are necessary for KRAS-driven lung tumorigenesis even when LKB1 expression is silenced. Intriguingly, treatment of mice bearing established KRAS^{G12C}-driven lung tumors with single agent DCC-3116 decreased tumor burden, further demonstrating that ULK-mediated autophagy may be important for maintenance of KRAS^{G12C}-driven lung tumors. Although we and others have demonstrated that autophagy inhibition as a monotherapy modestly reduces tumor burden in some preclinical models[11,43], this has not been recapitulated in human cell line-derived models or in clinical trials with HCQ. This could be attributed to the relatively low potency of autophagy inhibition with HCQ, the low mutational burden of tumors arising in GEM models compared to human cancers or the use of non-specific autophagy inhibitors[53–55]. Indeed, we did observe that DCC-3116 treatment modestly inhibited the growth of one human KRAS^{G12C} mutant lung cancer cell line, NCI-H358, both *in vitro* and *in vivo*, suggesting that ULK1/2 inhibition as a monotherapy may indeed have significant single agent activity in certain settings.

In addition to assessment of preclinical therapeutic responses in GEM models, this study also addressed the histopathology of KRAS^{G12C}-driven lung tumors, either in combination with LKB1 silencing or expression of dominant-negative TP53^{R172H}, in GEM models. In both the KRAS^{G12C}/LKB1^{Null} and KRAS^{G12C}/TP53^{R172H} GEM models of lung tumorigenesis, we noted the outgrowth of atypical adenomatous hyperplasia (AAH) and adenocarcinomas as was reported for KRAS^{G12D}-driven lung tumors some years ago. Interestingly, KRAS^{G12C}/LKB1^{Null}-driven lung tumors also displayed mixed adeno/squamous carcinomas (ASC) and mucinous adenocarcinomas that were not observed in the KRAS^{G12C}/TP53^{R172H}-driven model. Analysis of the mucinous adenocarcinomas indicated that some tumor cells expressed the gastric lineage marker HNF4α, an observation originally reported in KRAS^{G12D}/NKX2.1^{Null}-driven lung tumors[40,56]. In this (and related) GEM model(s), silencing of NKX2.1, a master transcriptional regulator of both lung and thyroid development, promoted the transition of lung tumor cells to a mucinous gastric cell phenotype through the action of HNF4α in partnership with the FOXA1/2 transcription factors[56]. Interestingly, HNF4α expressing KRAS^{G12C}/LKB1^{Null}-driven lung tumor cells retained expression of NKX2.1 suggesting that NKX2.1 silencing is not required for the emergence of mucinous adenocarcinomas when LKB1 expression is silenced. Whether this reflects the ability of

LKB1 signaling to: 1. Regulate cancer metabolism through effects on triosephosphate isomerase (TPI) or altered lactate production and secretion; 2. Regulate transcription effects on histone acetylation via elevated CRTC2-CREB signaling downstream of the salt-inducible kinases (SIKs) or effects on HDAC1/3 or some other signaling circuit remains to be determined[57–62].

Finally, in both GEM models of $KRAS^{G12C}$-driven lung tumorigenesis, we observed inhibition of both AAH and adenocarcinoma with either single agent treatment or the combination of sotorasib plus DCC-3116. By contrast, in the GEM model of $KRAS^{G12C}$/$LKB1^{Null}$-driven lung tumorigenesis, we noted an enrichment of the mixed adeno-squamous and mucinous carcinomas after cessation of therapy. This suggests that this histopathological class of $KRAS^{G12C}$/$LKB1^{Null}$-driven lung tumors may be relatively resistant to agents such as sotorasib that covalently inhibit the inactive, GDP-bound state of $KRAS^{G12C}$. This could reflect: 1. Differences in expression of RGS GTPase-activating proteins (GAPs) that promote GTP hydrolysis by $KRAS^{G12C}$; A cell state transition that is less dependent on the $KRAS^{G12C}$ oncoprotein as has been described for resistance of EGFR-driven lung cancers to pathway-targeted inhibition of EGFR tyrosine kinase activity or; 3. Elevated expression of downstream factors such as c-MYC that we have recently shown can confer resistance to the combination of trametinib plus HCQ in models of KRAS-driven pancreatic cancer[6,63,64].

In closing, our data support the testing of ULK1/2 inhibitors in patients with KRAS-driven lung cancer, either as single agents or in combination with direct inhibitors of KRAS oncoproteins, or of KRAS-regulated signaling pathways downstream of KRAS such as the RAF>MEK>ERK MAP kinase pathway. It will be interesting to interrogate specimens from patients on such trials prior to and after the likely eventual emergence of drug resistance to determine the extent to which potential resistance mechanisms glimpsed in preclinical models are observed in clinical trials. Such observations may pave the way for more efficacious regimens of therapy that maximize the depth and durability of desirable anti-tumor effects while minimizing toxicity.

MATERIALS AND METHODS

Cell Culture: Cell lines were routinely tested for mycoplasma contamination. All human lung cancer cell lines were obtained from the ATCC and cultured in RPMI (Roswell Park Memorial Institute) 1640 (Gibco 11875-093) supplemented with 10%(v/v) fetal bovine serum (FBS) (Gibco 10438-026) and 1% penicillin plus streptomycin (P/S) (Gibco 15140-122). Mouse tumor-derived cell lines were derived as previously described. Briefly, lungs from tumor-bearing mice were homogenized in a solution of digestive enzymes and plated in dishes. Cells were harshly split to allow for the outgrowth of tumor cells. The specific genetic abnormalities in each cell line were confirmed by analysis of genomic DNA or by immunoblotting. All

mouse tumor-derived cell lines were cultured in DMEM/F12 (Dulbecco's Modified Eagle Medium F12) (Gibco 11330-032) with 10%(v/v) FBS and 1% P/S.

Fluorescent Autophagy Reporter (FAR): A vector encoding the chimeric FAR protein comprising mCherry:EGFP:LC3 was introduced into human and mouse cell lines as previously described with virus infected cells selected using puromycin and FAR expressing cells selected by flow cytometry.[8,34] To assess autophagy, FAR expressing cells were seeded at equal densities in 6-well plates. After 24 hours, media was replaced with media containing the various drug treatments for 48 hours. Cells were harvested and stained with 1mM SYTOX Blue (Invitrogen S34857) for the exclusion of dead cells. Flow cytometry (Beckman Coulter CytoFLEX) was performed to assess mCherry and EGFP intensity and quantify the mCherry:EGFP ratio normalized to dimethyl sulfoxide (DMSO) control. For statistical analysis, an ordinary one-way ANOVA and Dunnett's multiple comparisons test were performed.

Lentiviral Transduction: HEK293T cells (Table 1) were seeded 24 hours prior to transfection in DMEM/F12 (10% FBS 1% P/S). DNA for lentivirus generation was introduced into these cells using a Lipofectamine 3000 kit (Invitrogen L3000015). All virus-containing supernatants were filtered through 0.45mm filters before use. To increase the efficiency of infection, 10mg/mL of Polybrene (MilliporeSigma TR-1003-G) was supplemented in the virus-containing media when added to cells. Cells were selected for successful infection through antibiotic selection with the corresponding antibiotics (puromycin or blasticidin) or flow cytometry for fluorescent markers. All plasmids used are described in Table 1 and are commercially available or previously published except the pLV-ULK1^{K46N} plasmid.

ELISA assay for pS318-ATG13: pS318-ATG13 antibody (Rockland Immunochemicals, 600-401-C49) was biotinylated using a Biotin Labeling Kit-NH_2 (Dojindo, LK03). ELISA plates (Corning, 9018) were coated in anti-ATG13 antibody (Table 1) overnight at 4 degrees. Cells were plated in equal densities in a 96-well plate. After 24 hours, cells were treated with various drug treatments for 16 hours, washed with 1x Phosphate-Buffered Saline (PBS), and then lysed in M-Per lysis buffer (Thermo Fisher, 78501) supplemented with 1x Ethylenediaminetetraacetic acid (EDTA, Thermo Fisher, 1861274), 1x Sigma Phosphatase Inhibitor (Sigma, 5726), 2x Halt Phosphatase and Protease inhibitor Cocktail (Thermo Fisher, 78446) for 15 minutes on an orbital shaker at 4°C. Cell extracts were then centrifuged for 10 minutes at 4,000 rpm in a 4°C refrigerated centrifuge. ELISA assay plates were washed twice with 1x ELISA wash buffer (Biolegend, 421601), blocked for 1 hour at RT with 1x ELISA dilutant buffer (Biolegend Cat# 421203), then washed twice with 1x wash buffer. Cell extracts were diluted in wash buffer, incubated in the ELISA plate at room temperature for 2 hours and then washed twice with 1x wash buffer. The biotinylated pS318-ATG13 antibody was diluted in 1x dilutant buffer and added to each well. After 1 hour at room temperature, wells were washed twice with 1x well wash buffer. Streptavidin-Poly-HRP antibody

(Table 1) was diluted in 1x dilutant and added to each well for 1 hour at room temperature. Wells were washed twice with 1x well wash buffer and tetramethylbenzidine substrate (Biolegend, 421101) was added to each well for 15 minutes at room temperature. After 15 minutes, ELISA stop solution (Invitrogen, SS04) was added to each well. Background correction was performed by including control wells that received every reagent except for protein lysate and subtracting that value from all samples. Plates were immediately read on a Synergy HTX (BioTek) plate reader at 450nm and 540nm. Statistical analysis was performed using a one-way ANOVA with Tukey's multiple comparisons.

Immunoblotting: Cell extracts were harvested as previously described[7]. Following clearing by centrifugation, protein lysates were quantified using a bicinchoninic acid assay (BCA) (Thermo Scientific 23250). 20-50mg samples of cell extract were fractionated by SDS-PAGE and then western blotted onto nitrocellulose membranes. Membranes were probed with primary antibodies (Table 1) overnight at 4°C. Secondary antibodies (Table 1) were diluted and incubated at room temperature for one hour. Membranes were imaged and analyzed on an Odyssey® CLx Infrared Imaging System (LI-COR®) and analyzed using Image Studio Software (LI-COR®).

***In vitro* synergy assays:** Cells were seeded in triplicate at 5000-7000 cells/well into black-walled clear bottom 96-well plates (Costar 3603), cultured overnight in complete medium and then treated with various drug treatments at the indicated concentrations for 72 hrs. At the endpoint, ATP was quantified using CellTiter-Glo luminescent cell viability assay (Promega, G7570) per the manufacturer's instructions. Luminescence was measured using a BioTek Synergy HTX plate reader and data were normalized to untreated controls. Synergy was determined using ComBenefit software (HSA, Bliss, Loewe models).[65]

Live Cell Imaging: Cells were imaged using an Incucyte Zoom Live Cell Imager (Sartorius) over time and analyzed using the IncuCyte Analysis Software (Sartorius). Cells were seeded at equal densities in 6-well plates and treated with various inhibitors either as single agents or in combination and imaged every two hours. Media was replaced after 48 hours for each well. Percent confluence and standard error was calculated at each time point. Statistical analysis was performed using a one-way ANOVA with Tukey's multiple comparisons.

Generation of pLV-ULK^{K46N} expression. vector: The pLV-ULK1^{K46N} plasmid was designed and constructed by VectorBuilder. 3x HA-tagged human ULK1^{K46N} was cloned into a pLV lentivirus backbone vector containing a tetracycline-inducible promoter including a Tet response element and puromycin resistance cassette synthesized.

Animal Work: All animal work was approved by the Institutional Care and Use Committees at the University of Utah (protocol #: 21-1005). All work containing biohazardous agents was approved by the

University of Utah Biosafety Committee. Mice were fed *ad libitum,* housed in micro isolator cages, and monitored daily in a temperature-controlled environment with a twelve-hour light/dark cycle. *Kras*$^{LSL\text{-}G12C}$ and Lkb1$^{fl/fl}$ mice were purchased from The Jackson Laboratory (Table 1)[24,66]. All mice were on a mixed genetic background. Both female and male mice were used for all experiments. Experimental adult mice were initiated between 6-8 weeks of age through nasal inhalation of adenovirus expressing CMV-Cre recombinase (Table 1) using $5x10^7$ pfu per mouse as previously described[67]. Lung tumorigenesis was monitored in live mice with micro-computed tomography (microCT) scans (Perkin Elmer Quantum Gx) with a Cu 0.06+ Al 0.5 X-ray filter, 72 mm acquisition, and 45 mm reconstitution for a 2-minute standard scan. Mice were scanned up to 9 times (<1 gray of total radiation). Mice on treatment were weighed 2-3x per week and euthanized if unacceptable weight loss (>20%) was observed. Upon euthanasia, lungs were dissected and fixed using standard protocols[68]. For xenograft models, Nod.Cg-Prkdcscid/J mice were purchased from Jackson Laboratories (Table 1) or generated in-house. Cell lines were injected sub-cutaneously into the flank of adult mice at $1\text{-}5x10^6$ cells per injection in a 1:1 mixture of serum-free Opti-MEM (Gibco, 31985-070) and Matrigel (Corning, 356231). Once tumors were palpable, they were measured using digital calipers. Once tumors reached ~$250mm^3$ mice were randomized to treatment arms. Mice were treated for 28 days or until maximum tumor volume was reached (~$1cm^3$). Tumor volume was calculated as equal to (tumor length) x (tumor width^2)/2). Statistical analysis on xenograft assays was performed using an ordinary one-way ANOVA and unpaired student's t-test. Corn oil vehicle (Sigma C8261) and sotorasib treatments were administered once daily via oral gavage. DCC-3116 was formulated in chow, and mice were fed *ad libitum*. Schematics illustrating treatment strategies were created using BioRender.

Survival of mice on treatment: *KL* mice were randomized to treatment arms at 10 weeks post tumor initiation (p.i.) and treated every day or until euthanasia end-point criteria were reached or after a pre-determined 56 days of drug treatment. Euthanasia criteria were defined per IACUC protocol to monitor pain and distress symptoms in mice[69]. Statistical analysis of survival was performed using the Log-rank (Mantel-Cox) test.

Tissue hematoxylin and eosin, immunohistochemistry staining: Lungs were harvested and inflated by perfusion through the trachea with 5 mLs of 10%(v/v) buffered formalin (Epredia 5725), and then fixed overnight with gentle rocking at RT following standard protocols[68]. Fixed lungs were embedded in paraffin and then 5mm sections were prepared. Harris hematoxylin acidified (Epredia 6765003) and Eosin Y (Epredia 71211) stains were performed on all tissue sections. For immunohistochemistry (IHC), sections were first deparaffinized using standard protocols, and antigen retrieval was performed in a pressure cooker using 1x Citrate Buffer pH6 (Novus Biologicals, NB90062075). IHC was performed using the ImmPRESS® Polymer Reagents (Vector Laboratories). Primary antibodies (Table 1) were diluted and

incubated at room temperature for 1 hour and then counter-stained with hematoxylin. Sections were dehydrated using standard protocols and mounted with ClearVue Mountant (Epredia 4212). Alcian Blue - Periodic Acid Schiff (PAS) staining was performed using standard protocols. Briefly, slides were deparaffinized, rehydrated and incubated in Alcian Blue (Leica 38016SS3A). Slides were washed and incubated in periodic acid (Leica 38016SS4A) followed by the Schiff Reagent (Fisher SS32-500).

Tissue Imaging and Quantification: All tissue imaging was performed using a 3D-Histech Midi Panoramic Scanner (Epredia) at 20x magnification. Tumor burden was quantified using CaseViewer software (Epredia). Total lung area and tumor area were digitally annotated using a closed polygon annotation. Total tumor and lung areas were summed, and the percent tumor burden was calculated. Immunohistochemical quantification was performed using 3D-Histech Quant Center software (Epredia) as previously described (Silvis et al. 2023). Statistical analysis was performed using an unpaired Student's t-test.

Inhibitor Treatments: All pathway-targeted inhibitors (Table 1) were obtained from reputable sources and resuspended in the appropriate solvent (DMSO or water) for *in vitro* testing. The biochemical activity of all compounds was tested *in vitro* before being used *in vivo*. Compounds for *in vivo* dosing were resuspended in 10%(v/v) DMSO and 90%(v/v) corn oil (Table 1) or formulated in mouse chow. The DCC-3116 formulated mouse chow (Research Diets) was formulated with an OpenStandard Diet with 15% Kcal% Fat and 360 mg DCC-3116. CL/kg Diet.

TABLE 1: Reagent Table

Reagent type (species) or resource	Designation	Source or Reference	Identifiers	Additional Information
Genetic reagent (*Mus musculus*)	*Kras*$^{LSL-G12C}$	The Jackson Laboratory PMID: 32792368	Strain #:033068	Dow Lab
Genetic reagent (*Mus musculus*)	*Stk11*$^{fl/fl}$ (Mouse gene is *Stk11* and protein is referred to as LKB1)	The Jackson Laboratory PMID: 21124450	Strain #:014143	Morrison Lab
Genetic reagent (*Mus musculus*)	*Trp53*$^{wm-R172H}$	PMID: 30262850		Lozano Lab
Genetic reagent *(Mus musculus)*	Nod.Cg-Prkdcscid/J	The Jackson Laboratory	Strain #:001303	
Adenovirus	Ad5-CMV-CRE	University of Iowa Viral Vector Core	VVC-U of Iowa-5	
Cell Line *(Homo sapiens)*	293T	ATCC	CRL-3216	
Cell Line *(Homo sapiens)*	NCI-H2122	ATCC	CRL-5985	
Cell Line *(Homo sapiens)*	Calu-1	ATCC	HTB-54	
Cell Line *(Homo sapiens)*	NCI-H358	ATCC	CRL-5807	
Cell Line *(Homo sapiens)*	NCI-H23	ATCC	CRL-5800	
Cell Line *(Homo sapiens)*	Cor-L23	Sigma-Aldrich	92031919	
Cell Line *(Mus musculus)*	KL70	Tumor-derived cell line		
Antibody	Mouse monoclonal anti-β-Actin	Cell Signaling Technology	Cat# 3700	WB (1:10,000)
Antibody	Rabbit monoclonal anti-phospho-AKT S473	Cell Signaling Technology	Cat# 4060	WB (1:1,000) IHC (1:100)
Antibody	Mouse monoclonal anti-Akt	Cell Signaling Technology	Cat#2920	WB (1:1,000)
Antibody	Rabbit monoclonal anti-phospho AMPKa S485	Cell Signaling Technology	Cat# 2537	WB (1:1,000)
Antibody	Rabbit monoclonal anti-phospho AMPKa T172	Cell Signaling Technology	Cat# 2535	WB (1:1,000)

Antibody	Rabbit monoclonal anti-AMPK	Cell Signaling Technology	Cat# 5831	WB (1:1,000)
Antibody	Rabbit polyclonal anti-phospho-ATG13 S318	Rockland Immunochemicals	Cat# 600-401-C49	ELISA (1:500)
Antibody	Rabbit monoclonal anti-ATG13	Cell Signaling Technology	Cat# 13272	ELISA (1:500)
Antibody	Rabbit monoclonal anti-HNF4α	Cell Signaling Technology	Cat# 3113	IHC (1:500)
Antibody	Rabbit monoclonal anti-LKB1 (IHC formulated)	Cell Signaling Technology	Cat# 13031	IHC (1:250)
Antibody	Rabbit monoclonal anti-LKB1	Cell Signaling Technology	Cat# 3050	WB (1:1,000)
Antibody	Rabbit monoclonal anti-NKX2.1	Abcam	Cat# ab76013	IHC (1:2,000)
Antibody	Mouse monoclonal anti-p44/p42 ERK1/2	Cell Signaling Technology	Cat# 4696	WB (1:1,000)
Antibody	Rabbit monoclonal anti-phospho-p44/42 Thr202/Tyr204 ERK1/2	Cell Signaling Technology	Cat# 4377	WB (1:1,000) IHC (1:600)
Antibody	Rabbit polyclonal anti-TP53	Leica Biosystems	NCL-L-p53-CM5p	IHC (1:1,000) WB (1:2,000)
Antibody	Rabbit monoclonal anti-Pro-Surfactant Protein C (pSPC)	Millipore Sigma	Cat# AB3786	IHC (1:2,000)
Antibody	Rabbit monoclonal anti-RAS	Cell Signaling Technology	Cat#	WB (1:1,000)
Antibody	Streptavidin-Poly-HRP antibody	Thermo Fisher	Cat# 21140	ELISA (1:4,000)
Antibody	Rabbit monoclonal anti-phospho-ULK1 S555	Cell Signaling Technology	Cat# 5869	WB (1:500)
Antibody	Rabbit monoclonal-phospho-ULK1 S757	Cell Signaling Technology	Cat# 14202	WB (1:500)
Antibody	Rabbit monoclonal-ULK1	Cell Signaling Technology	Cat# 8054	WB (1:500)
Antibody	IRDye 800 CW Goat anti-Rabbit IgG	LI-COR	Cat# 926-32211	WB (1:20,000)
Antibody	IRDye 680LT Donkey anti-Mouse IgG	LI-COR	Cat# 926-68022	WB (1:20,000)
Recombinant DNA reagent	pCW57-MCS1-P2A-MSC2 (Blast)	Addgene	Plasmid # 80921	
Recombinant DNA reagent	psPAX2	Addgene	Plasmid # 12260	
Recombinant DNA reagent	pMD2.G	Addgene	Plasmid # 12259	
Recombinant DNA reagent	pLV-ULK1^{K46N}	Vector Builder		
Recombinant DNA reagent	pBabePuro:mCherry-GFP-LC3	Addgene	Plasmid # 22418	

Recombinant DNA reagent	pUltra-Hot	Addgene	Plasmid # 24130	
Chemical compound, drug	sotorasib	Deciphera Pharmaceuticals		
Chemical compound, drug	DCC-3116	Deciphera Pharmaceuticals		
Chemical compound, drug	DCC-3116 formulated chow	Deciphera Pharmaceuticals, Research Diets		
Chemical compound	Trametinib	Shanghai Biochem Partner	Cat# BCP02307	
Chemical compound, vehicle	Corn oil	Sigma-Aldrich	Cat # C8267	
Chemical compound	DMSO	Sigma-Aldrich	Cat# D8418	

ACKNOWLEDGEMENTS

We want to acknowledge the members of the McMahon and Kinsey labs for their valuable support, guidance, and sharing of reagents. P. Ghazi was supported by a JEDI award from the Life Sciences Editors Foundation, and we graciously thank Li-Kuo Su for editing suggestions and advice. The content is solely the responsibility of the authors and does not necessarily represent the official views of the National Institutes of Health.

This work was supported by the University of Utah Flow Cytometry Facility and the National Cancer Institute (NCI) through award number P30 CA042014. P. Ghazi would like to acknowledge funding provided by NCI under award number F31 CA261116. M. McMahon would like to acknowledge funding provided by NCI under award numbers R01 CA131261, R01 CA176839, and P30 CA042014, the Five for the Fight, the Huntsman Cancer Foundation, and the Huntsman Lung Cancer Disease Center. C. Kinsey would like to acknowledge funding provided by NCI award number K08 CA230151, the Huntsman Cancer Foundation, and the V Foundation Clinical Scholar Award. E. Snyder would like to acknowledge funding provided by the NCI under award numbers R01 CA212415, R01 CA240317 and R01 CA237404. G. Lozano would like to acknowledge funding provided by the NCI under award number R01 CA82577.

Disclosures: Research described here was supported through a Sponsored Research Agreement between the University of Utah and Deciphera Pharmaceuticals and awarded to M.M and C.G.K. M.M has previously but no longer been retained as a paid consultant to Deciphera Pharmaceuticals; C.G.K

reported personal fees from Deciphera Pharmaceuticals outside the submitted work. M.B and D.L.F are stockholders of Deciphera Pharmaceuticals. No other disclosures were reported.

REFERENCES

1. Riely, G. J. *et al.* Frequency and distinctive spectrum of KRAS mutations in never smokers with lung adenocarcinoma. *Clin Cancer Res* **14**, 5731–4 (2008).
2. Ahrendt, S. A. *et al.* Cigarette smoking is strongly associated with mutation of the K-ras gene in patients with primary adenocarcinoma of the lung. *Cancer* **92**, 1525–30 (2001).
3. Uprety, D. & Adjei, A. A. KRAS: From undruggable to a druggable Cancer Target. *Cancer Treat Rev* **89**, 102070 (2020).
4. Ostrem, J. M., Peters, U., Sos, M. L., Wells, J. A. & Shokat, K. M. K-Ras(G12C) inhibitors allosterically control GTP affinity and effector interactions. *Nature* **503**, 548–51 (2013).
5. Janes, M. R. *et al.* Targeting KRAS Mutant Cancers with a Covalent G12C-Specific Inhibitor. *Cell* **172**, 578-589.e17 (2018).
6. Silvis, M. R. *et al.* MYC-mediated resistance to trametinib and HCQ in PDAC is overcome by CDK4/6 and lysosomal inhibition. *J Exp Med* **220**, (2023).
7. Truong, A. *et al.* Chloroquine Sensitizes GNAQ/11-mutated Melanoma to MEK1/2 Inhibition. *Clin Cancer Res* **26**, 6374–6386 (2020).
8. Kinsey, C. G. *et al.* Protective autophagy elicited by RAF→MEK→ERK inhibition suggests a treatment strategy for RAS-driven cancers. *Nat Med* **25**, 620–627 (2019).
9. Bryant, K. L. *et al.* Combination of ERK and autophagy inhibition as a treatment approach for pancreatic cancer. *Nat Med* **25**, 628–640 (2019).
10. Li, T.-T. & Zhu, H.-B. LKB1 and cancer: The dual role of metabolic regulation. *Biomed Pharmacother* **132**, 110872 (2020).
11. Bhatt, V. *et al.* Inhibition of autophagy and MEK promotes ferroptosis in Lkb1-deficient Kras-driven lung tumors. *Cell Death Dis* **14**, 61 (2023).
12. Shackelford, D. B. *et al.* LKB1 inactivation dictates therapeutic response of non-small cell lung cancer to the metabolism drug phenformin. *Cancer Cell* **23**, 143–58 (2013).
13. Sanchez-Cespedes, M. The role of LKB1 in lung cancer. *Fam Cancer* **10**, 447–53 (2011).
14. Blumenschein, G. R. *et al.* A randomized phase II study of the MEK1/MEK2 inhibitor trametinib (GSK1120212) compared with docetaxel in KRAS-mutant advanced non-small-cell lung cancer (NSCLC). *Annals of Oncology* **26**, 894–901 (2015).
15. Mohsen, S. *et al.* Autophagy Agents in Clinical Trials for Cancer Therapy: A Brief Review. *Current Oncology* **29**, 1695–1708 (2022).
16. Takeda, K., Kaisho, T. & Akira, S. Toll-like receptors. *Annu Rev Immunol* **21**, 335–76 (2003).
17. Al-Bari, M. A. A. Chloroquine analogues in drug discovery: new directions of uses, mechanisms of actions and toxic manifestations from malaria to multifarious diseases. *J Antimicrob Chemother* **70**, 1608–21 (2015).
18. Seglen, P. O., Grinde, B. & Solheim, A. E. Inhibition of the lysosomal pathway of protein degradation in isolated rat hepatocytes by ammonia, methylamine, chloroquine and leupeptin. *Eur J Biochem* **95**, 215–25 (1979).
19. Mauthe, M. *et al.* Chloroquine inhibits autophagic flux by decreasing autophagosome-lysosome fusion. *Autophagy* **14**, 1435–1455 (2018).
20. Yang, A. *et al.* Autophagy Sustains Pancreatic Cancer Growth through Both Cell-Autonomous and Nonautonomous Mechanisms. *Cancer Discov* **8**, 276–287 (2018).
21. Glick, D., Barth, S. & Macleod, K. F. Autophagy: cellular and molecular mechanisms. *J Pathol* **221**, 3–12 (2010).

22. Zachari, M. & Ganley, I. G. The mammalian ULK1 complex and autophagy initiation. *Essays Biochem* **61**, 585–596 (2017).
23. Lee, M. J., Park, J.-S., Jo, S. Bin & Joe, Y. A. Enhancing Anti-Cancer Therapy with Selective Autophagy Inhibitors by Targeting Protective Autophagy. *Biomol Ther (Seoul)* **31**, 1–15 (2023).
24. Zafra, M. P. *et al.* An In Vivo Kras Allelic Series Reveals Distinct Phenotypes of Common Oncogenic Variants. *Cancer Discov* **10**, 1654–1671 (2020).
25. Zhu, L., Jiang, L., Yang, J., Gu, W. & He, J. Clinical characteristics and prognosis of patients with lung adenosquamous carcinoma after surgical resection: results from two institutes. *J Thorac Dis* **10**, 2397–2402 (2018).
26. Li, C. & Lu, H. Adenosquamous carcinoma of the lung. *Onco Targets Ther* **11**, 4829–4835 (2018).
27. Canon, J. *et al.* The clinical KRAS(G12C) inhibitor AMG 510 drives anti-tumour immunity. *Nature* **575**, 217–223 (2019).
28. Fell, J. B. *et al.* Identification of the Clinical Development Candidate MRTX849, a Covalent KRASG12C Inhibitor for the Treatment of Cancer. *J Med Chem* **63**, 6679–6693 (2020).
29. Hallin, J. *et al.* The KRASG12C Inhibitor MRTX849 Provides Insight toward Therapeutic Susceptibility of KRAS-Mutant Cancers in Mouse Models and Patients. *Cancer Discov* **10**, 54–71 (2020).
30. Awad, M. M. *et al.* Acquired Resistance to KRASG12C Inhibition in Cancer. *New England Journal of Medicine* **384**, 2382–2393 (2021).
31. Zhao, Y. *et al.* Diverse alterations associated with resistance to KRAS(G12C) inhibition. *Nature* **599**, 679–683 (2021).
32. Blaquier, J. B., Cardona, A. F. & Recondo, G. Resistance to KRASG12C Inhibitors in Non-Small Cell Lung Cancer. *Front Oncol* **11**, 787585 (2021).
33. Tanaka, N. *et al.* Clinical Acquired Resistance to KRASG12C Inhibition through a Novel KRAS Switch-II Pocket Mutation and Polyclonal Alterations Converging on RAS-MAPK Reactivation. *Cancer Discov* **11**, 1913–1922 (2021).
34. Kimura, S., Noda, T. & Yoshimori, T. Dissection of the autophagosome maturation process by a novel reporter protein, tandem fluorescent-tagged LC3. *Autophagy* **3**, 452–60 (2007).
35. Wang, Y. *et al.* Global profiling of AMG510 modified proteins identified tumor suppressor KEAP1 as an off-target. *iScience* **26**, 106080 (2023).
36. Hara, T. *et al.* FIP200, a ULK-interacting protein, is required for autophagosome formation in mammalian cells. *J Cell Biol* **181**, 497–510 (2008).
37. Nakada, D., Saunders, T. L. & Morrison, S. J. Lkb1 regulates cell cycle and energy metabolism in haematopoietic stem cells. *Nature* **468**, 653–8 (2010).
38. Lang, G. A. *et al.* Gain of function of a p53 hot spot mutation in a mouse model of Li-Fraumeni syndrome. *Cell* **119**, 861–72 (2004).
39. Moisés, J. *et al.* NKX2-1 expression as a prognostic marker in early-stage non-small-cell lung cancer. *BMC Pulm Med* **17**, 197 (2017).
40. Snyder, E. L. *et al.* Nkx2-1 represses a latent gastric differentiation program in lung adenocarcinoma. *Mol Cell* **50**, 185–99 (2013).
41. Mason, R. J. & Dobbs, L. G. 8 - Alveolar Epithelium and Pulmonary Surfactant. in *Murray and Nadel's Textbook of Respiratory Medicine (Sixth Edition)* (eds. Broaddus, V. C. et al.) 134-149.e5 (W.B. Saunders, Philadelphia, 2016). doi:https://doi.org/10.1016/B978-1-4557-3383-5.00008-7.
42. Guo, J. Y. *et al.* Autophagy suppresses progression of K-ras-induced lung tumors to oncocytomas and maintains lipid homeostasis. *Genes Dev* **27**, 1447–1461 (2013).

43. Bhatt, V. *et al.* Autophagy modulates lipid metabolism to maintain metabolic flexibility for Lkb1-deficient Kras-driven lung tumorigenesis. *Genes Dev* **33**, 150–165 (2019).
44. Khayati, K. *et al.* Autophagy compensates for Lkb1 loss to maintain adult mice homeostasis and survival. *Elife* **9**, (2020).
45. Poillet-Perez, L. *et al.* Autophagy maintains tumour growth through circulating arginine. *Nature* **563**, 569–573 (2018).
46. Rao, S. *et al.* A dual role for autophagy in a murine model of lung cancer. *Nat Commun* **5**, 3056 (2014).
47. Johnson, K. A. Imaging techniques for small animal imaging models of pulmonary disease: micro-CT. *Toxicol Pathol* **35**, 59–64 (2007).
48. Pons-Tostivint, E., Lugat, A., Fontenau, J.-F., Denis, M. G. & Bennouna, J. STK11/LKB1 Modulation of the Immune Response in Lung Cancer: From Biology to Therapeutic Impact. *Cells* **10**, (2021).
49. Li, J. *et al.* Regulation and function of autophagy in pancreatic cancer. *Autophagy* **17**, 3275–3296 (2021).
50. Ashrafi, A. *et al.* Current Landscape of Therapeutic Resistance in Lung Cancer and Promising Strategies to Overcome Resistance. *Cancers (Basel)* **14**, (2022).
51. Sanchez-Cespedes, M. *et al.* Inactivation of LKB1/STK11 is a common event in adenocarcinomas of the lung. *Cancer Res* **62**, 3659–62 (2002).
52. Caiola, E. *et al.* Co-occurring KRAS mutation/LKB1 loss in non-small cell lung cancer cells results in enhanced metabolic activity susceptible to caloric restriction: an in vitro integrated multilevel approach. *J Exp Clin Cancer Res* **37**, 302 (2018).
53. Wolpin, B. M. *et al.* Phase II and pharmacodynamic study of autophagy inhibition using hydroxychloroquine in patients with metastatic pancreatic adenocarcinoma. *Oncologist* **19**, 637–8 (2014).
54. Mancias, J. D. & Kimmelman, A. C. Targeting autophagy addiction in cancer. *Oncotarget* **2**, 1302–6 (2011).
55. Amaravadi, R. K., Kimmelman, A. C. & Debnath, J. Targeting Autophagy in Cancer: Recent Advances and Future Directions. *Cancer Discov* **9**, 1167–1181 (2019).
56. Camolotto, S. A. *et al.* FoxA1 and FoxA2 drive gastric differentiation and suppress squamous identity in NKX2-1-negative lung cancer. *Elife* **7**, (2018).
57. Stein, B. D. *et al.* LKB1-Dependent Regulation of TPI1 Creates a Divergent Metabolic Liability between Human and Mouse Lung Adenocarcinoma. *Cancer Discov* **13**, 1002–1025 (2023).
58. Eichner, L. J. *et al.* HDAC3 is critical in tumor development and therapeutic resistance in Kras-mutant non-small cell lung cancer. *Sci Adv* **9**, eadd3243 (2023).
59. Hollstein, P. E. *et al.* The AMPK-Related Kinases SIK1 and SIK3 Mediate Key Tumor-Suppressive Effects of LKB1 in NSCLC. *Cancer Discov* **9**, 1606–1627 (2019).
60. Shackelford, D. B. & Shaw, R. J. The LKB1-AMPK pathway: metabolism and growth control in tumour suppression. *Nat Rev Cancer* **9**, 563–75 (2009).
61. Qian, Y. *et al.* MCT4-dependent lactate secretion suppresses antitumor immunity in LKB1-deficient lung adenocarcinoma. *Cancer Cell* **41**, 1363-1380.e7 (2023).
62. Compton, S. E. *et al.* LKB1 controls inflammatory potential through CRTC2-dependent histone acetylation. *Mol Cell* **83**, 1872-1886.e5 (2023).
63. Li, C. *et al.* The G protein signaling regulator RGS3 enhances the GTPase activity of KRAS. *Science* **374**, 197–201 (2021).
64. Sequist, L. V *et al.* Genotypic and histological evolution of lung cancers acquiring resistance to EGFR inhibitors. *Sci Transl Med* **3**, 75ra26 (2011).

65. Di Veroli, G. Y. *et al.* Combenefit: an interactive platform for the analysis and visualization of drug combinations. *Bioinformatics* **32**, 2866–8 (2016).
66. Nakada, D., Saunders, T. L. & Morrison, S. J. Lkb1 regulates cell cycle and energy metabolism in haematopoietic stem cells. *Nature* **468**, 653–8 (2010).
67. Fasbender, A. *et al.* Incorporation of adenovirus in calcium phosphate precipitates enhances gene transfer to airway epithelia in vitro and in vivo. *J Clin Invest* **102**, 184–93 (1998).
68. Limjunyawong, N., Mock, J. & Mitzner, W. Instillation and Fixation Methods Useful in Mouse Lung Cancer Research. *J Vis Exp* e52964 (2015) doi:10.3791/52964.
69. Ullman-Culleré, M. H. & Foltz, C. J. Body condition scoring: a rapid and accurate method for assessing health status in mice. *Lab Anim Sci* **49**, 319–23 (1999).

Figure 1:

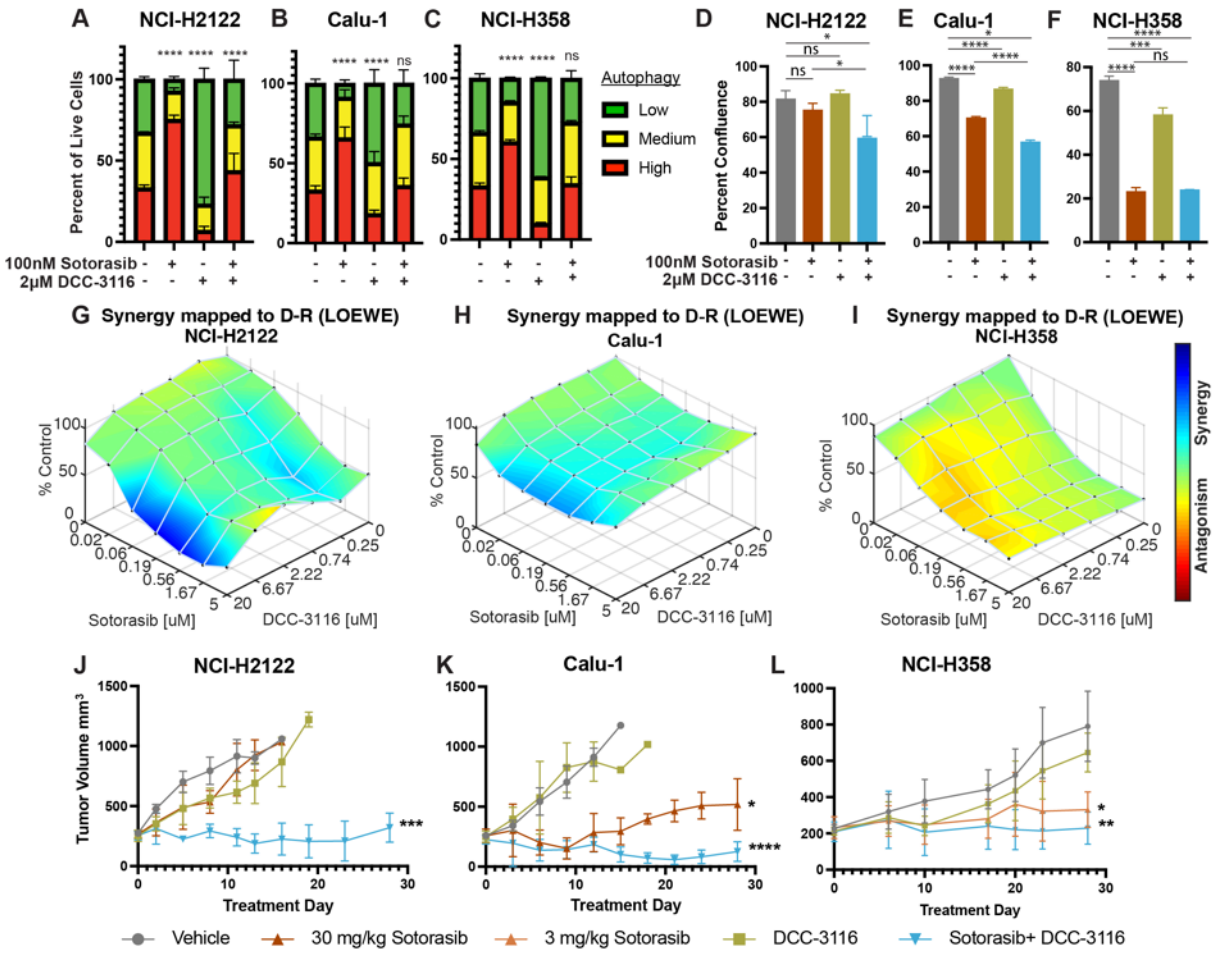

Fig. 1: Human KRAS^{G12C}-driven lung cancer cells are sensitive to co-inhibition of KRAS^{G12C} and ULK1/2.

A-C, Human KRAS^{G12C}-driven cell lines NCI-H2122 (A), Calu-1 (B) and NCI-H358 (C) increase autophagy as assessed by mCherry-EGFP-LC3 reporter after 48 hours of sotorasib treatment and decrease autophagy after 48h hours of DCC-3116 treatment. Red=high autophagy, Yellow= medium autophagy, Green= low autophagy. Statistical significance was determined by comparing autophagic flux levels to DMSO control. Ns= not significant, *p<0.05 **p<0.01 ***p<0.001 ****p<0.0001.

D-F, Quantification of percent confluence of human KRAS^{G12C}-driven cell lines at 72 hours post-drug treatment.

G-I, *In vitro* synergy assay of human KRAS^{G12C}-driven cell lines using the Loewe method after 72 hours of treatment.

J-L, Tumor volume measured over 28 days of treatment in mice inoculated with NCI-H2122 (J), Calu-1 (K) and NCI-H358 (L) cells. Vehicle and sotorasib were administered once daily via oral gavage and DCC-3116 was formulated in the chow.

Figure 2:

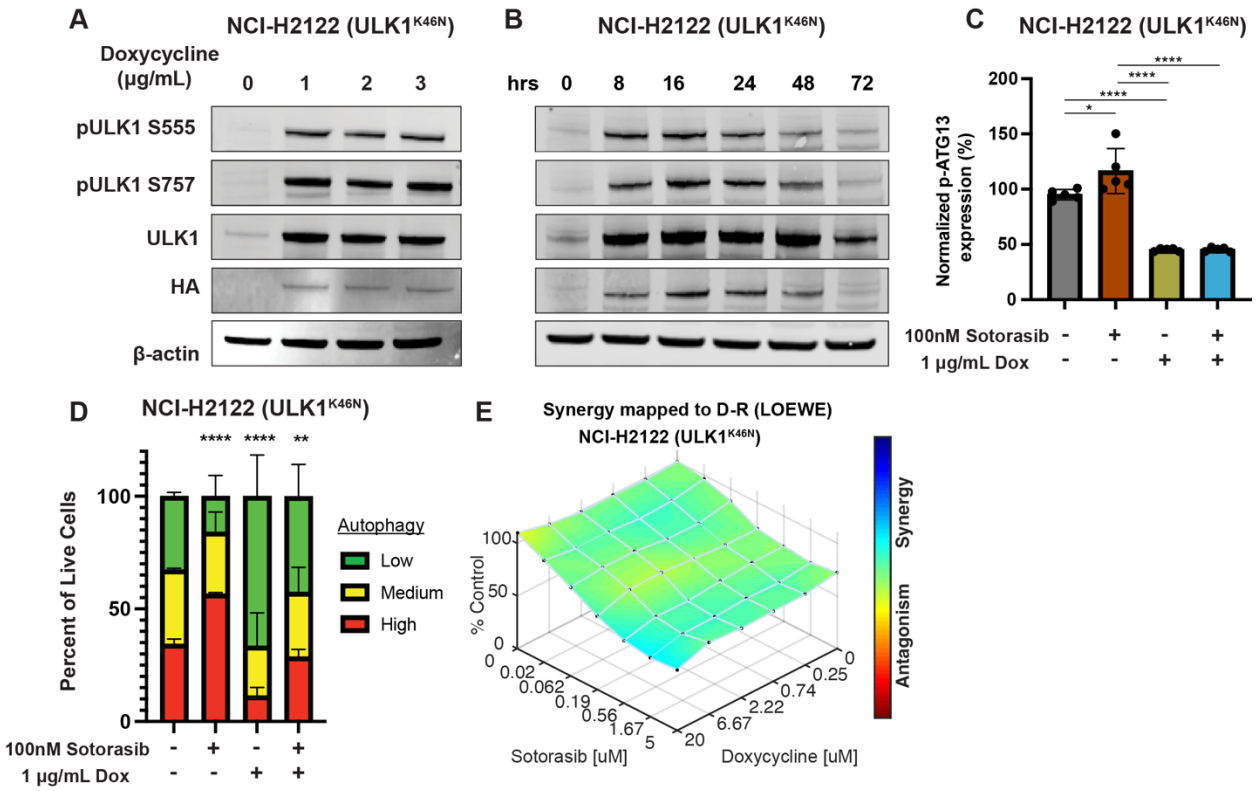

Fig. 2: Genetic inhibition of ULK1 decreases autophagy and cooperates with sotorasib to reduce cell viability.

A, Immunoblot of NCI-H2122:ULK1^{K46N} cells after 24 hours of doxycycline treatment.

B, Immunoblot of NCI-H2122:ULK1^{K46N} cells treated with 1 ug/mL doxycycline over time (hours).

C, ELISA assay of pS318-ATG13 expression after 16 hours of doxycycline treatment. N=3.

D, NCI-H2122:ULK1^{K46N} cells were engineered to express the mCherry-EGFP-LC3 reporter, and a decrease in autophagy was demonstrated after 48 hours of doxycycline treatment. N=3. All statistical significance was performed with an ordinary one-way ANOVA with Dunnett's multiple comparisons test. *p<0.05 **p<0.01 ***p<0.001 ****p<0.0001

E, Synergy analysis of NCI-H2122:ULK1^{K46N} cells treated with DMSO control, sotorasib and/or doxycycline over 48 hours.

Figure 3:

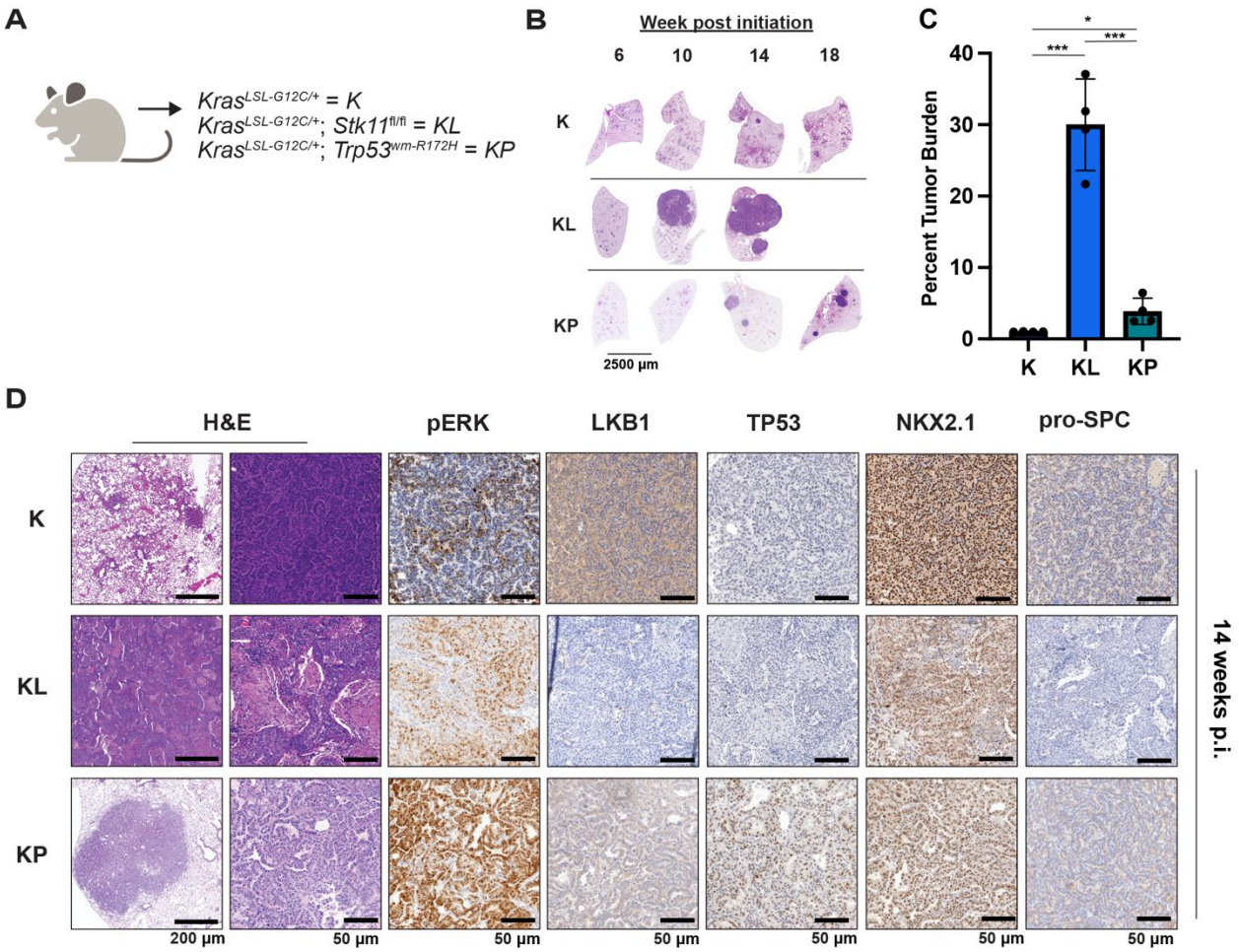

Fig. 3: Either LKB1 silencing or expression of dominant-negative TP53^{R172H} cooperates with KRAS^{G12C} in GEM models of lung cancer.

A, Schematic of genotypes of GEM models and abbreviations.

B, Representative images of lung lobes from GEM models at indicated time points post-initiation of lung tumorigenesis.

C, Quantification of lung tumor burdens from GEM models 14 weeks post-initiation of tumorigenesis. N= 3-4

D, Hematoxylin and eosin (H&E) and immunohistochemical analysis of representative lung sections from GEM models 14 weeks post-initiation of tumorigenesis. p.i.=post initiation.

Figure 4:

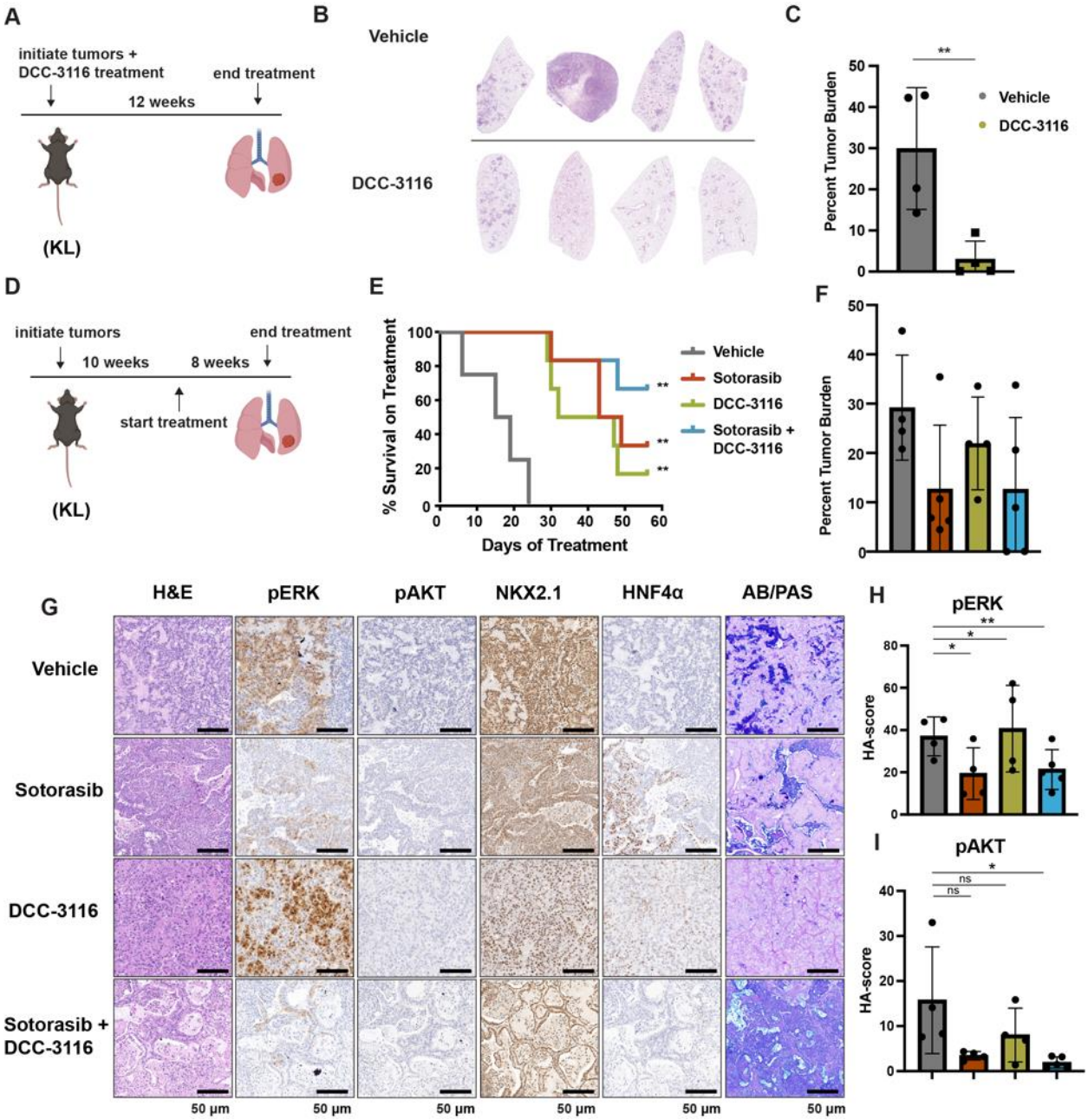

Fig. 4: Combined inhibition of KRAS^{G12C} and ULK1/2 decreases tumor initiation and increases survival in *KL* GEMMs.

A, Schematic of lung tumor prevention dosing strategy of KL GEMMs. DCC-3116 was administered in drug-formulated chow. N=4

B, Representative images of lung lobes from GEMMs 12 weeks post-initiation of tumorigenesis and DCC-3116 treatment.

C, Quantification of tumor burden of (B).

D, Schematic of treating tumor-bearing KL mice with vehicle control, 30 mg/kg sotorasib, chow containing DCC-3116 or the combination. DCC-3116 was administered in drug-formulated chow. Mice were treated every day for 56 days or until termination criteria were reached, whichever was reached first. N=4-6.

E, Kaplan-Meyer survival curve of survival on treatment of KL mice treated as indicated. Statistical analysis was performed using a Log-Rank test. **p<.01

F, Quantification of tumor burden of (E).

G, H&E analysis of representative lung sections from KL mice after treatment. AB/PAS= Alcian Blue Periodic Acid Schiff, for staining mucins.

H-I, Quantification of immunohistochemical staining of treated mice pERK (H) and pAKT (I) *p<0.05 **p<0.01 ns= not significant

Figure 5:

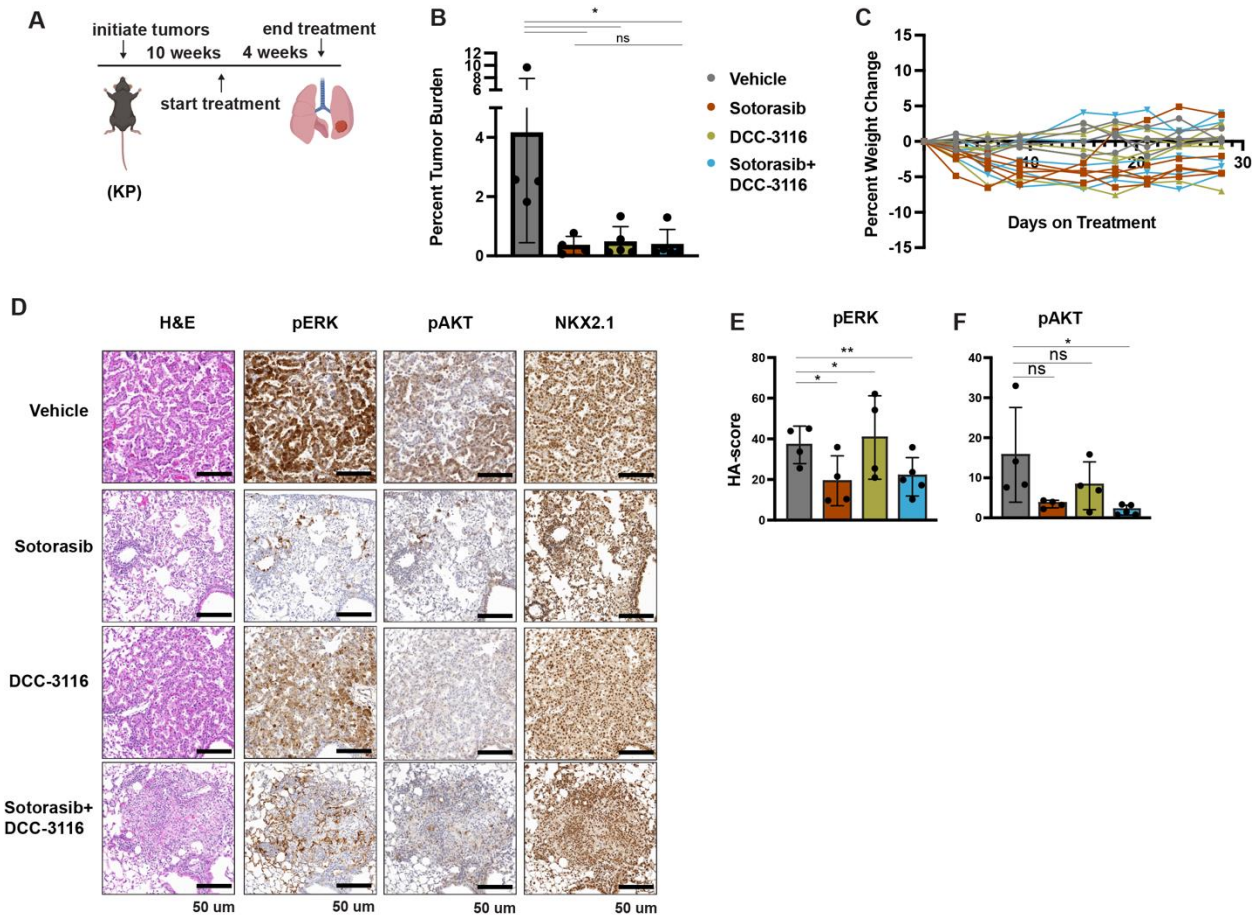

Fig. 5: Inhibition of KRAS^{G12C} and ULK1/2 reduces tumor burden in a *KP* GEM models

A, Schematic of the treatment of *KP* GEM models. Mice were administered vehicle control or 30 mg/kg sotorasib once daily via oral gavage. DCC-3116 was administered in drug-formulated chow. N=4-5

B, Quantification of tumor burden of mice after 4 weeks of treatment. *p<0.05 ns=not significant.

C, Percent change in the body weight of mice on treatment over 4 weeks.

D, Representative images of histological analysis of lung lobes from *KP* mice 4 weeks after treatment.

E-F, Quantification of immunohistochemical staining of treated mice pERK1/2 (E) and pAKT1-3 (F) *p<0.05 **p<0.01 ns= not significant

Figure 6:

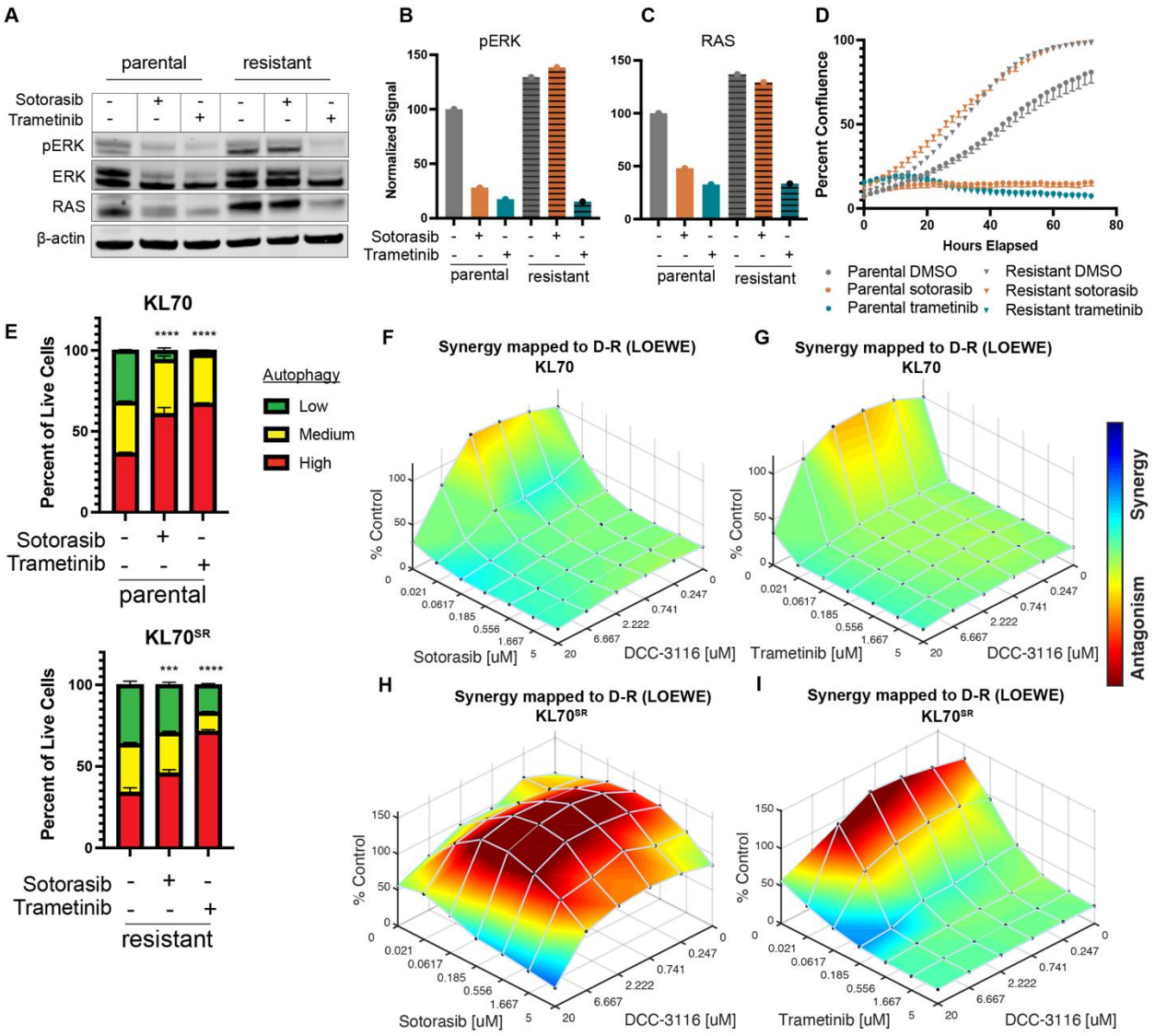

Fig. 6 *KL* lung-cancer-derived cells that acquire resistance to sotorasib increase RAS and pERK1/2 expression and do not increase autophagy after sotorasib treatment.

A, Immunoblot analysis of KL.70 and KL.70^{R} cells treated with 100nM sotorasib or 100nM trametinib after 48 hours of treatment.

B-C, Quantification of signal from A normalized to b-actin. D, Live cell imaging of percent confluence of KL.70 cells over time treated with DMSO, 100nm sotorasib of 100nM trametinib.

E, Autophagy measurement with FAR reporter in cells assessed by mCherry-eGFP-LC3 reporter after 48 hours of 100nM sotorasib or 100nM trametinib treatment. Red=high autophagy, Yellow= medium autophagy, Green= low autophagy. Ns= not significant, *p<0.05 **p<0.01 ***p<0.001 ****p<0.0001.

F-G, Cell viability assay of KL.70 cells treated with indicated compounds at indicated doses after 72 hours of treatment.

H-I, Cell viability assay of KL.70^{R} cells treated with indicated compounds at indicated doses after 72 hours of treatment.

Supplemental Figure 1:

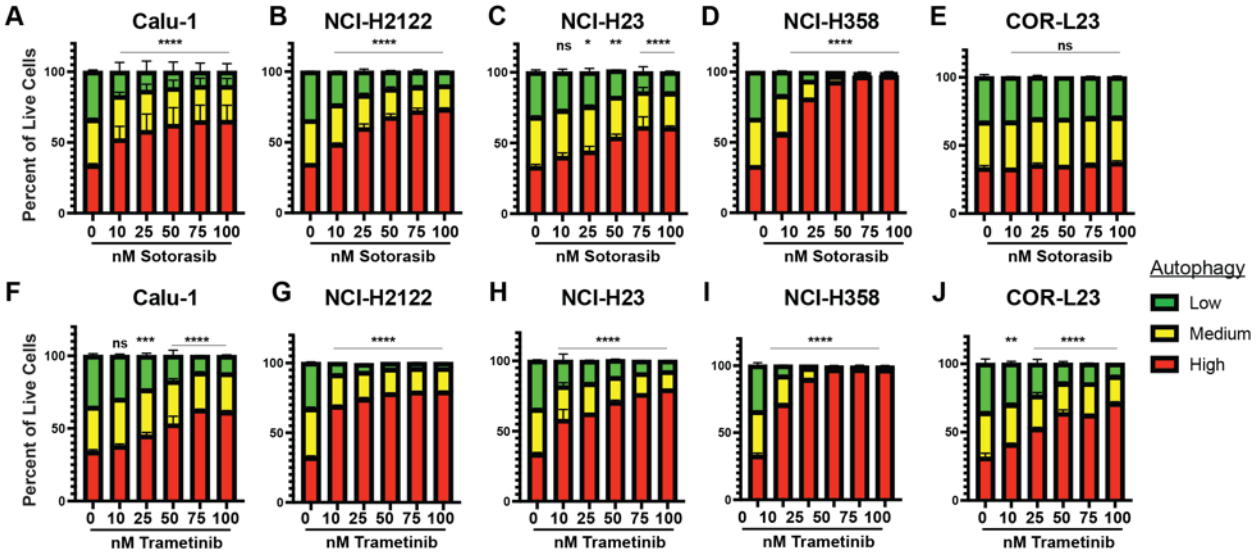

Fig. S1. Human KRAS-driven lung cancer cells increase autophagy after KRAS^{G12C} or MEK inhibition.

A-E, Autophagy levels in human KRAS^{G12C}-driven lung cancer cells Calu-1 (A), NCI-H2122 (B), NCI-H23 (C), NCI-H358 (D) and the KRAS^{G12V}-driven human lung cancer cell line Cor-L23 (E) after 48 hours of sotorasib at indicated concentrations with the FAR reporter. Red=high autophagy, Yellow= medium autophagy, Green= low autophagy. ns= not significant, *p<0.05 **p<0.01 ***p<0.001 ****p<0.0001.

F-J, Autophagy levels in human KRAS^{G12C}-driven lung cancer cells Calu-1 (F), NCI-H2122 (G), NCI-H23 (H), NCI-H358 (I) and the KRAS^{G12V}-driven human lung cancer cell line Cor-L23 (J) after 48 hours of trametinib at indicated concentrations with the FAR reporter. Red=high autophagy, Yellow= medium autophagy, Green= low autophagy. ns= not significant, *p<0.05 **p<0.01 ***p<0.001 ****p<0.0001.

Supplemental Figure 2:

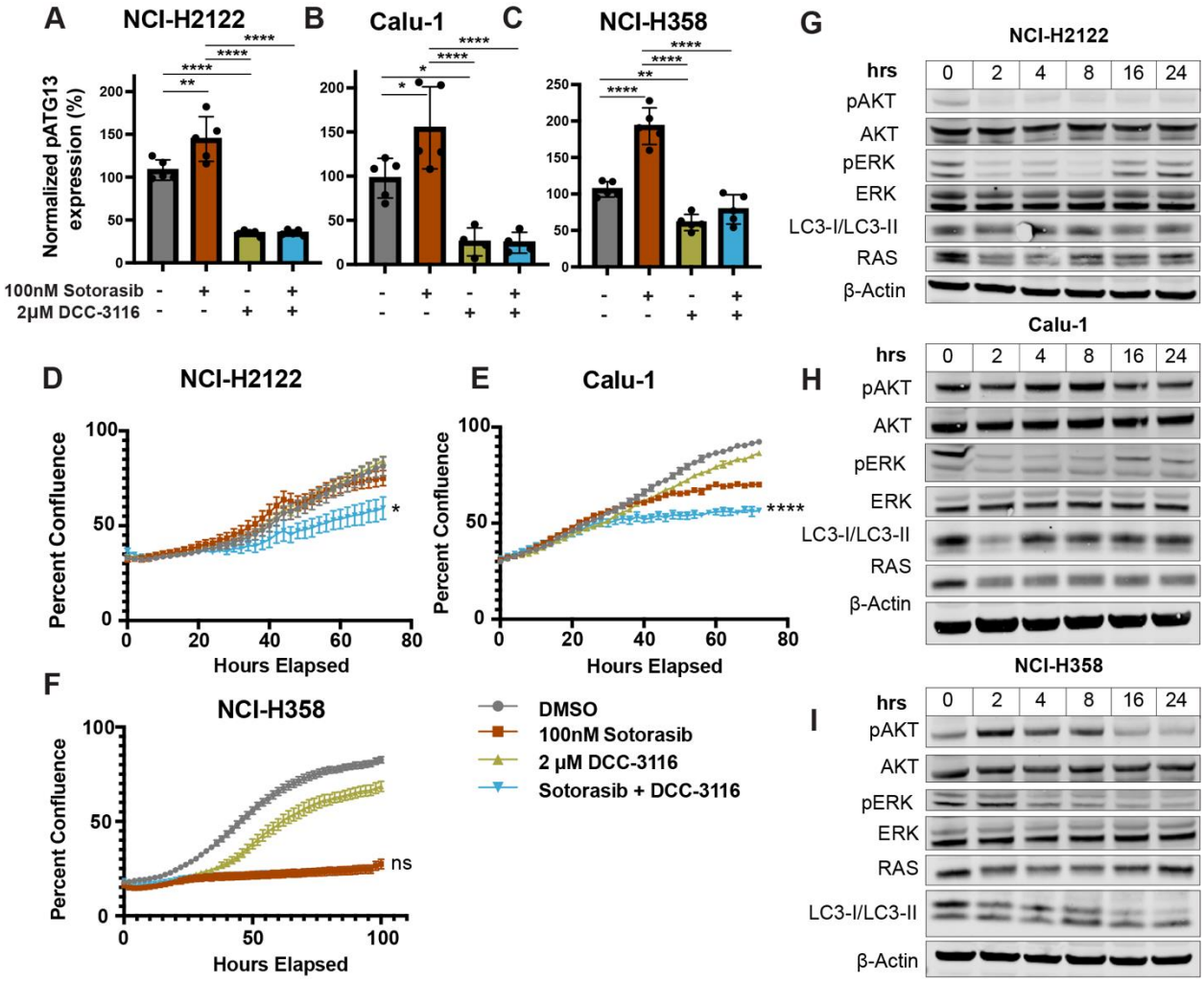

Fig. S2. Human KRAS^{G12C}-driven lung cancer cell lines increase autophagy and decrease cellular proliferation after sotorasib treatment.

A-C, ELISA measurement of pS318-ATG13 signal after 16 hours of drug treatment in NCI-H2122 (A), Calu-1 (B) and NCI-H358 cell lines (C). N=3. Statistical analysis was performed using an ordinary one-way ANOVA with Tukey's multiple comparisons test. ns= not significant, *p<0.05 ****p<0.0001.

D-F, Percent confluence over time of NCI-H2122 (D), Calu-1 (E) and NCI-H358 (F) cell lines treated with indicated compounds over time. Statistical analysis was performed using an ordinary one-way ANOVA with Tukey's multiple comparisons test. ns= not significant, *p<0.05 **p<0.01 ***p<0.001 ****p<0.0001

G-I, Immunoblotting analysis of NCI- H2122 (G), Calu-1 (H), and NCI-H358 (I) cell lines after 100nM sotorasib treatment over 24 hours.

Supplemental Figure 3:

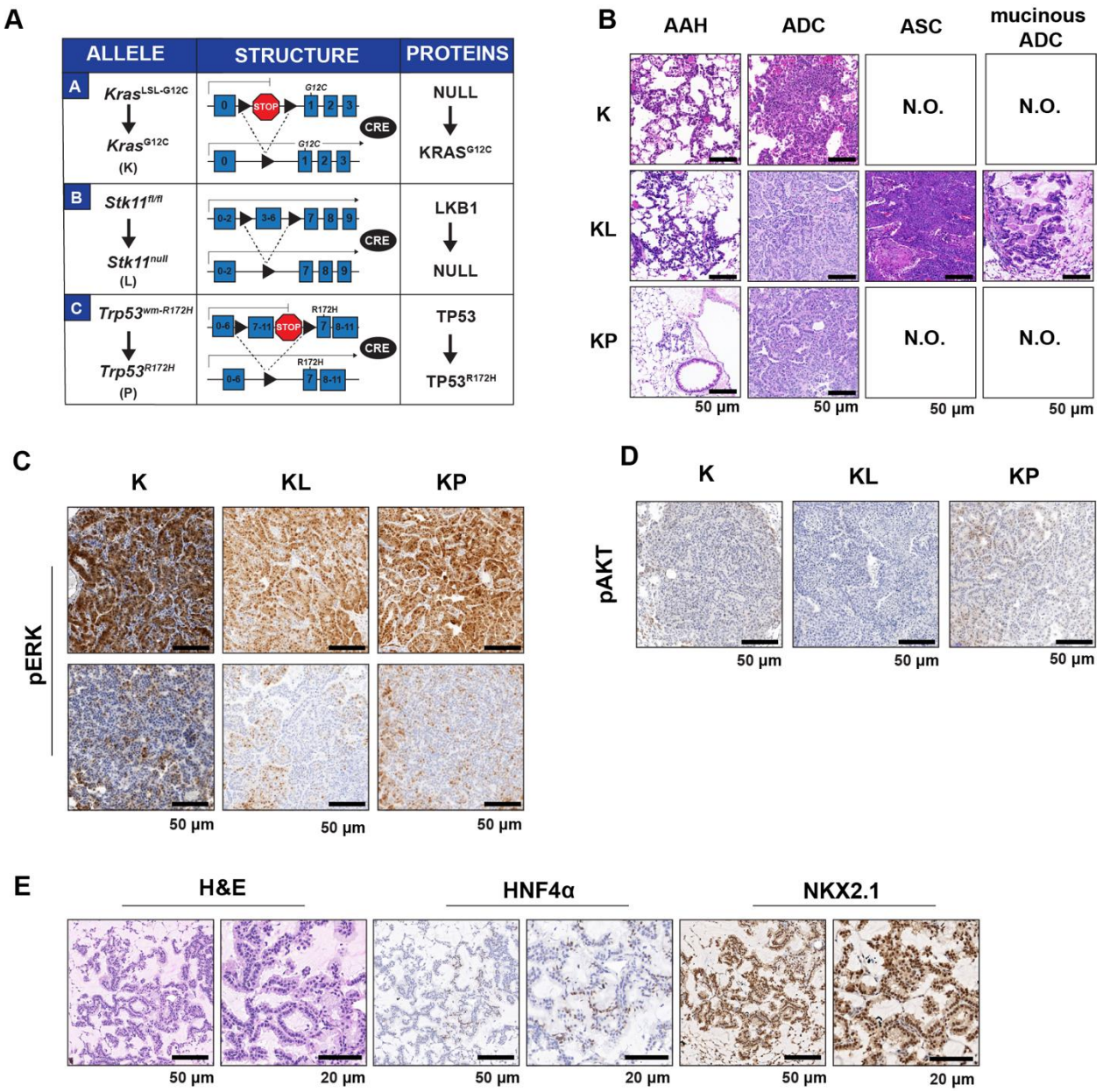

Fig. S3 Loss of LKB1 expression leads to mixed ASC and mucinous ADC lung tumors in KRAS^{G12C}-driven GEMMs.

A, Schematic of allele, structure, and protein changes in GEM models used.

B, Representative hematoxylin and eosin stains of K, KL and KP GEM models 14 weeks post-initiation. N.O.= not observed, AAH= atypical adenomatous hyperplasia, ADC= adenocarcinoma, ASC= adeno/squamous cell carcinoma, mucinous ADC= mucinous adenocarcinoma.

C-D, Representative immunohistochemical stains of pERK1/2 (C) and pAKT1-3 (D) signal in *K*, *KL* and *KP* GEMMs.

E, Representative images of hematoxylin and eosin (H&E) staining and immunohistochemistry of indicated proteins.

Supplemental Figure 4:

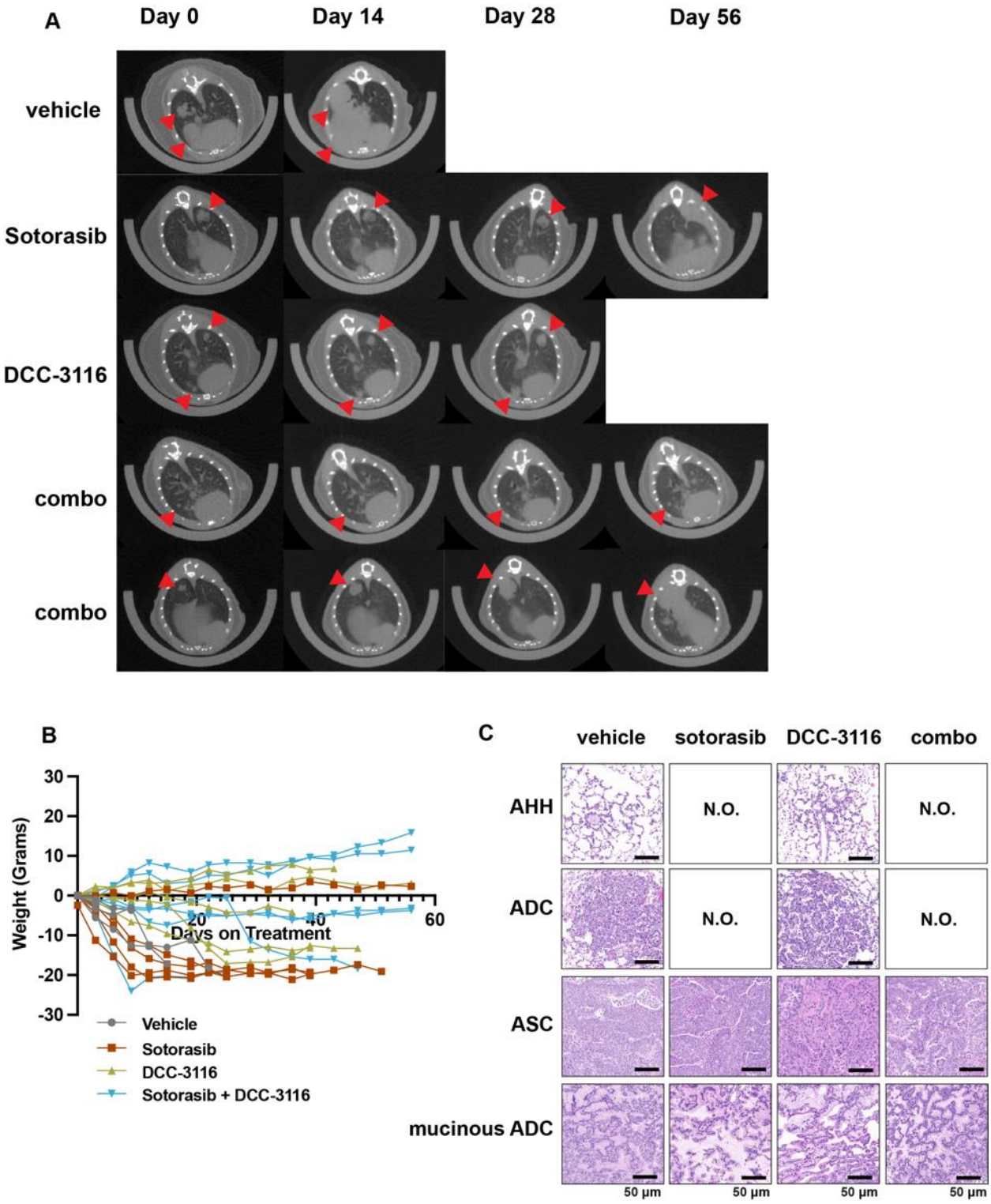

Fig. S4 MicroCT, body weight and pathological analysis of treated KL mice.

A, Representative microCT images of KL mice pre-treatment (Day 0) and 14 days, 28 days and 56 days post-treatment. Vehicle-treated mice and most DCC-3116 treated mice reached termination criteria before the 56-day endpoint. Red arrows indicate lung tumors.

B, Percent change in the body weight of mice over the course of the treatment period.

C, Representative images of hematoxylin and eosin staining of lung sections of KL mice at the end of treatment. N.O.= not observed, AH= alveolar hyperplasia, ADC= adenocarcinoma, ASC= adenocarcinoma/squamous cell carcinoma, mucinous ADC= mucinous adenocarcinoma.

Supplemental Figure 5:

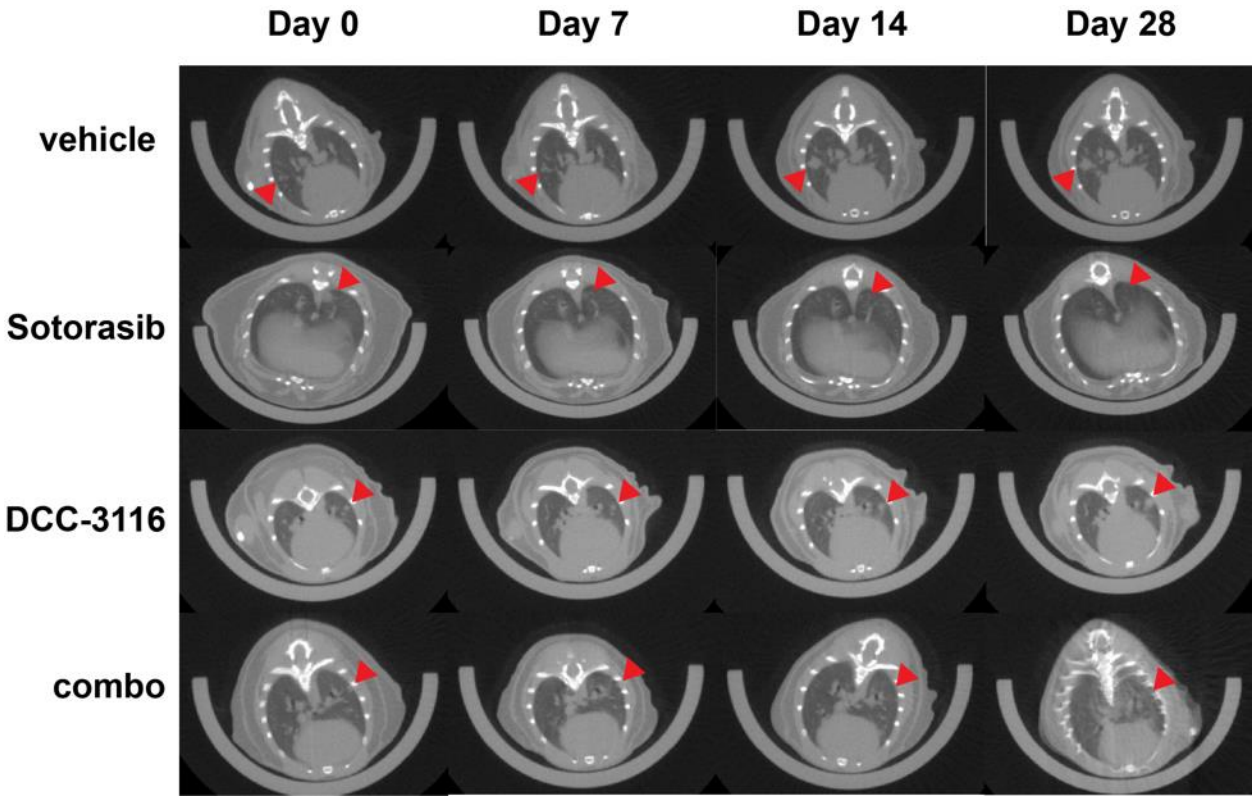

Fig. S5 MicroCT images of KP mice on treatment.

Representative microCT images of KP mice pre-treatment (Day 0) and 7 days, 14 days and 28 days post-treatment. Red arrows indicate lung tumors.